A Conjugate Gradient FFT Method for the Computation of the Scattering by Thin Planar Material Plates

April 1988

T. J. Peters and J. L. Volakis
Radiation Laboratory
Dept. of Electrical Engineering and Computer Science
The University of Michigan
1301 Beal Avenue
Ann Arbor, MI 48109-2122

Technical Report No. 389604-2-T

Prepared for

General Dynamics
Fort Worth Division
P. O. Box 748
Fort Worth, Texas 76101

Abstract

A conjugate gradient FFT formulation and implementation of the scattering by planar material plates is presented. The plates considered are of arbitrary material composition and periphery. A substantial part of this investigation concentrated on the development of efficient and higher accuracy FFT algorithms. This resulted in the generation of a scattering code 3 to 4 times faster than the traditional and, in addition, a higher convergence was achieved with the incorporation of basic functions for the representation of the plate's current density.

TABLE OF CONTENTS

		Page #
CHAPTER I.	INTRODUCTION	1
	Motivation	1
	Literature Review	1
	Objectives	2
CHAPTER II.	DERIVATION OF THE CONJUGATE GRADIENT METHOD	4
	Introduction	4
	Derivation	5
	Typical Operator Equations	11
CHAPTER III.	DERIVATION AND COMPUTATION OF A DISCRETE FOURIER TRANSFORM USING HIGHER ORDER INTEGRATION AND PRIME FACTORIZATION	13
	Introduction	13
	Derivation of a DFT	13
	Higher Order Integration	18
	Derivation of a Prime Factor FFT	26
	Extension to Two Dimensions	32
	Test Results	34
CHAPTER IV.	SCATTERING FROM A SINGLE PLANAR PLATE	37
	Orientation	37
	Integral Equations	38
	Surface Generator	42
	Perfectly Conducting Plate	43
	Thin Dielectric Plate	45
	Thin Dielectric and Magnetic Plate	47
	Calculation of Radar Cross Section	52
CHAPTER V.	RESULTS	54
CHAPTER VI.	FUTURE WORK	65

CHAPTER I

INTRODUCTION

1.1 Motivation

The material plate scattering problem is one of the most commonly occurring scattering phenonena which does not have a known analytic solution. Many practical electrically thin structures have edges and corners which provide a significant contribution to the scattered fields. For electrically large surfaces the scattering contributions due to edges and corners are fairly localized so that computation of the surface currents and scattered fields from plates will give much insight on the scattering behavior of more arbitrary shapes.

One on the prime reasons for studying the scattering characteristics of material plates is to understand how the material distribution effects the scattered fields. Not only is it important to know the scattered fields but it is also desirable to know how to change the material composition of a scatterer to achieve a certain scattering characteristic.

1.2 Literature Review

At the present time efficiency is still a prime concern for numerical solution of scattering by material plates with above resonant dimensions. This efficiency is

measured in terms of minimizing computational factors such as time, storage and cost. The purpose of this study is to develop a method which has the potential to solve a wide class of scattering problems in an efficient manner. Newman et al [1] and Naor et al [2] treat rectangular material plates, however, the basis functions are inappropriate for curved perimeters and the boundary conditions employed are not valid at edge on incidence with H-polarization. Good results have been obtained for perfectly conducting plates by Glisson et al [3] and Rao et al [4] using triangular cells and linear basis functions. Unfortunately, these methods rely on matrix solutions which may become restrictive for a body of above resonant dimensions. Studies on perfectly conducting wire and plate scatterers by Sarkar et al [5] and work by Christodoulou et al [6] on meshes combine the method of conjugate gradients [7]-[10] with the FFT [11]-[12] to solve operator equations directly without storing a large matrix.

1.3 Objectives

The major goal of this study is to develop an efficient numerical modeling technique to solve for the induced current and the scattered field from a material plate illuminated by a plane wave. The technique involves combining a conjugate gradient (CG) method with a fast Fourier transform (FFT) to solve a set of coupled convolution integral equations.

Achieving an efficient algorithm requires a good understanding of both a conjugate gradient method and the computation of the FFT. Chapter II gives a complete derivation of a conjugate gradient method. Chapter III derives the discrete Fourier transform (DFT) from the continous Fourier transform and describes how computation may be accomplished using various integration formulas combined with the FFT. Chapter IV describes the single material plate which includes the zero thickness perfectly conducting plate, the electrically thin dielectric plate, and

the combination dielectric and magnetic plate. Chapter V gives some preliminary numerical results and chapter VI describes some future work which will be an extension of this study.

CHAPTER II

DERIVATION OF A CONJUGATE GRADIENT METHOD

Introduction

The conjugate gradient method seeks the solution to the operator equation

$$Az = b \tag{2.1}$$

where A is an operator which is assumed to be non-singular. In order to derive the solution technique the concept of an inner product must be discussed. Let $\langle f, g \rangle$ denote the inner product of the two functions $f = f_r + jf_i$ and $g = g_r + jg_i$. If the functions are continuous, then given a region $s \in R^2$ and real functions $f_{r,i}, g_{r,i} \in R^2$ a suitable inner product could be given as

$$\langle f, g \rangle = \iint_s f(x,y) g^*(x,y) w(x,y) ds \tag{2.2}$$

where $*$ denotes the complex conjugate and $w(x,y)$ is a real weight function. It is most common to define $w(x,y)$ as

$$w(x,y) = \begin{cases} 1 & \text{for differential operators} \\ \sum_{n=0}^{N-1} \sum_{m=0}^{M-1} \delta(x - m\Delta x, y - n\Delta y) & \text{for integral operators} \end{cases} \tag{2.3}$$

If the functions are discrete $n \times 1$ vectors such that $f = [f_0\ f_1\ f_2\ \ldots\ f_{N-1}]^T$ and $g = [g_0\ g_1\ g_2\ \ldots\ g_{N-1}]^T$ a suitable inner product could be given as

$$\langle f, g \rangle = \sum_{n=0}^{N-1} g_n^* f_n. \tag{2.4}$$

Closely related to the inner product is the Euclidean norm of a function defined by

$$||f||_2 = \sqrt{\langle f, f \rangle}. \tag{2.5}$$

Another concept that must be introduced is the adjoint operator of A denoted by A^a which satisfies the relation

$$\langle Ap, q \rangle = \langle p, A^a q \rangle \tag{2.6}$$

for any p and q.

Derivation

With an understanding of these concepts, the following observation may be made. The solution of (2.1) will yield the same solution as the minimum of some quadratic functional. That functional may be written as

$$\begin{aligned} I(z) &= \langle b - Az, b - Az \rangle \\ &= \langle Az, Az \rangle - \langle b, Az \rangle - \langle Az, b \rangle + \langle b, b \rangle \\ &= \langle Az, Az \rangle - \langle Az, b \rangle^* - \langle Az, b \rangle + \langle b, b \rangle \\ &= 2\left[\frac{1}{2}\langle Az, Az \rangle - Re\langle Az, b \rangle + \frac{1}{2}\langle b, b \rangle\right] \\ &= 2\left[\frac{1}{2}\langle z, A^a Az \rangle - Re\langle z, A^a b \rangle + \frac{1}{2}\langle b, b \rangle\right]. \end{aligned} \tag{2.7}$$

The method of conjugate gradients [7-10] is a general solution technique for minimizing I. Making the substitutions $B = A^a A$, $h = A^a y$ and noting that the

solution is independent of the multiplicative factor 2 and the constant $\langle b, b\rangle$ the solution $z = A^{-1}b = B^{-1}h$ also minimizes the function $F(z)$ given by

$$F(z) = \frac{1}{2}\langle Bz, z\rangle - Re\langle h, z\rangle. \tag{2.8}$$

If A is non-singular then B will have the following properties [13].

1. Hermitian $B = B^a$
2. positive definite $\langle Bz, z\rangle > 0 \qquad z \neq 0$
3. eigenvalues are positive and real and
   eigenvectors are orthogonal

The solution is assumed to have the recursive form

$$z_{k+1} = z_k + \alpha_k p_k \tag{2.9}$$

where α_k is a real positive constant and p_k is called the search vector. This yields an expression for the residual r_{k+1} defined by

$$\begin{aligned} r_{k+1} &= h - Bz_{k+1} \\ &= h - B(z_k + \alpha_k p_k) \\ &= r_k - \alpha_k B p_k. \end{aligned} \tag{2.10}$$

Substituting (2.9) into (2.8)

$$F(z_{k+1}) = F(z_k) + \frac{1}{2}\alpha_k^2\langle Bp_k, p_k\rangle - \alpha_k Re\langle r_k, p_k\rangle. \tag{2.11}$$

To minimize this function with respect to α_k set

$$\frac{\partial}{\partial \alpha_k} F = 0 \tag{2.12}$$

and solve for

$$\alpha_k = \frac{Re\langle r_k, p_k\rangle}{\langle Bp_k, p_k\rangle}. \tag{2.13}$$

Substituting (2.13) into (2.11)

$$F(z_{k+1}) = F(z_k) - \frac{1}{2}\frac{(Re\langle r_k, p_k\rangle)^2}{\langle Bp_k, p_k\rangle}. \tag{2.14}$$

The function decreases at each step if $Re\langle r_k, p_k\rangle \neq 0$ and B is positive definite. However, $||b - Az||_2$ may not decrease at each step since it is not the function to be minimized. This local minimization does not guarantee that the solution is obtained in a finite number of steps. The crux of the conjugate gradient method is that global minimization in a finite number of steps may be achieved if the search vectors p_k are chosen correctly. In order to choose p_k it is informative to view the minimization from a geometric point of view. The vector p_k is a direction in n-space. The residual vector r_{k+1} is proportional to the difference between the exact solution and the $k+1$ approximation. Thus

$$\begin{aligned} r_{k+1} &= h - Bz_{k+1} \\ &= B(z - z_{k+1}) \end{aligned} \tag{2.15}$$

where z is the true solution

$$z = \left[z^1 \;\; z^2 \;\; z^3, \ldots, z^n\right]^T. \tag{2.16}$$

If p_k is chosen such that $\langle r_{k+1}, p_k\rangle = 0$ then the minimization occurs in an n-dimensional plane and since

$$\begin{aligned} \langle r_{k+1}, p_k\rangle &= 0 \\ &= \langle r_k - \alpha_k Bp_k, p_k\rangle \\ &= \left(r_k - \frac{Re\langle r_k, p_k\rangle}{\langle Bp_k, p_k\rangle} Bp_k\right) \\ &= \langle r_k, p_k\rangle - Re\langle r_k, p_k\rangle \end{aligned} \tag{2.17}$$

the inner product $\langle r_k, p_k\rangle$ is real. Thus $\langle r_{k+1}, p_k\rangle$ is recognized as the equation of an n-dimensional plane given by

$$\langle B(z - z_{k+1}), p_k\rangle = 0 \tag{2.18}$$

which may be rewritten as

$$\gamma_1 z^1 + \gamma_2 z^2 + \gamma_3 z^3 + \ldots + \gamma_n z^n = \beta_1 \tag{2.19}$$

which establishes the relationship between a linear equation and an n-dimensional plane. This idea may be extended to a system of equations by noting that the solution of a system of m $\leq$ n equations in n unknowns is the same as finding the intersection of m n-dimensional planes. With this in mind it can be surmised that if the search directions were generated such that $\langle r_{k+1}, p_s \rangle = 0$ for $s = 1, \ldots, k$ then at the kth iterative step the function would be minimized over the intersection of k planes. Another interpretation is that at each iteration a least squares solution is found to a system of m equations in n unknowns. The iterative nature of the solution stems from the fact that at each step the order of the leasts squares solution is increased and a more accurate solution is obtained. Criteria for chosing p_k may be found by expanding the product of the residual and all previous search directions.

$$\begin{aligned}
\langle r_{k+1}, p_{k-1} \rangle &= \langle r_k, p_{k-1} \rangle - \alpha_k \langle B p_k, p_{k-1} \rangle \\
\langle r_{k+1}, p_{k-2} \rangle &= \langle r_{k-1}, p_{k-2} \rangle - \alpha_{k-1} \langle B p_{k-1}, p_{k-2} \rangle - \alpha_k \langle B p_k, p_{k-2} \rangle \\
\langle r_{k+1}, p_{k-3} \rangle &= \langle r_{k-2}, p_{k-3} \rangle - \alpha_{k-2} \langle B p_{k-2}, p_{k-3} \rangle - \alpha_{k-1} \langle B p_{k-1}, p_{k-3} \rangle - \alpha_k \langle B p_k, p_{k-3} \rangle \\
&\vdots \\
\langle r_{k+1}, p_{k-n} \rangle &= -\sum_{s=0}^{n-1} \alpha_{k-s} \langle B p_{k-s}, p_{k-n} \rangle
\end{aligned} \tag{2.20}$$

Observation of (2.20) indicates that if the method is to reach an exact solution in n iterations, the condition

$$\langle B p_k, p_s \rangle = 0 \qquad s = 0, \ldots, k-1 \tag{2.21}$$

must be enforced. Equation (2.21) is recognized as the condition for the vectors p_k to be "B-orthogonal" or "mutually conjugate". Vectors with this property may

be generated by the Gram-Schmidt process. Given a set of linearly independent vectors $v_1, \ldots, v_n$ a set of "B-orthogonal" vectors may be generated as

$$\begin{aligned} p_1 &= v_1 \\ p_2 &= v_2 - b_{11}p_1 \\ p_3 &= v_3 - b_{21}p_1 - b_{22}p_2 \\ &\vdots \\ p_{k+1} &= v_{k+1} - \sum_{s=1}^{k} \beta_{ks} p_s \end{aligned} \tag{2.22}$$

where

$$\beta_{ks} = \frac{\langle Bv_{k+1}, p_s \rangle}{\langle Bp_s, p_s \rangle}. \tag{2.23}$$

Note that this method requires k matrix vector products for the kth iteration so it is inherently very inefficient for large k. However, if the vectors v_k are chosen to be the residuals r_k then all $\beta_{ks} = 0$ for $s = 1, \ldots, k-1$ which leaves only one matrix vector product per iteration. To show this, the relationship between residuals must be established. Taking the adjoint of (2.22) and multiplying by the residual r_c yields

$$\langle r_c, p_{k+1} \rangle = \langle r_c, r_{k+1} \rangle - \sum_{s=1}^{k} \beta_{ks} \langle r_c, p_s \rangle. \tag{2.24}$$

When $c = k+1$ the products $\langle r_c, p_s \rangle = 0$ for $s < c$ by virtue of (2.21) which implies

$$\langle r_{k+1}, p_{k+1} \rangle = \langle r_{k+1}, r_{k+1} \rangle \tag{2.25}$$

and for $c = k+2, \ldots, n$

$$\langle r_c, p_{k+1} \rangle = \langle r_c, r_{k+1} \rangle = 0. \tag{2.26}$$

Therefore, the residual vectors are orthogonal such that for $k \neq s$

$$\langle r_s, r_k \rangle = 0. \tag{2.27}$$

With (2.27) established take the inner product of r_{k+1} with (2.10) and observe that

$$-\frac{1}{\alpha_s} \langle r_{k+1}, r_{s+1} - r_s \rangle = \langle B^a r_{k+1}, p_s \rangle = \langle B r_{k+1}, p_s \rangle = 0 \tag{2.28}$$

for $s = 1, \ldots, k-1$ and

$$-\frac{\langle r_{k+1}, r_{k+1}\rangle}{\alpha_k} = \langle Br_{k+1}, p_k\rangle \tag{2.29}$$

for $s = k$. Thus $\beta_{ks} = 0$ for $s = 1, \ldots, k-1$.

The computations will be minimized if the search directions p_k are normalized with respect to $\langle r_k, r_k\rangle$. The algorithm, which will be referred to by this author as the "nested operator" algorithm, is expressed below.

initialize

$$r_1 = h - Bx_1 \tag{2.30}$$

$$\beta_0 = \frac{1}{\langle r_1, r_1\rangle} \tag{2.31}$$

$$p_1 = \beta_0 r_1 \tag{2.32}$$

for $k = 1, \ldots, n$

$$\alpha_k = \frac{1}{\langle Bp_k, p_k\rangle} \tag{2.33}$$

$$x_{k+1} = x_k + \alpha_k p_k \tag{2.34}$$

$$r_{k+1} = r_k - \alpha_k Bp_k \tag{2.35}$$

$$\beta_k = \frac{1}{\langle r_{k+1}, r_{k+1}\rangle} \tag{2.36}$$

$$p_{k+1} = p_k + \beta_k r_{k+1} \tag{2.37}$$

The algorithm is terminated at $k = n$ or when

$$\frac{||r_{k+1}||_2}{||h||_2} < \text{tolerance.} \tag{2.38}$$

Excluding the initialization, this algorithm requires one matrix vector product per iteration. The number of multiplications and divisions per iteration is $n^2 + 5n + 2$. However, the matrix B may or may not be explicitly known. In this case the residual expressed in (2.10) must be replaced by $A^a r$ with $r = b - Az$. The modified algorithm referred to by this author as the "split operator" algorithm is

initialize

$$r_1 = y - Ax_1 \tag{2.39}$$

$$\beta_0 = \frac{1}{\langle A^a r_1, A^a r_1 \rangle} \tag{2.40}$$

$$p_1 = \beta_0 A^a r_1 \tag{2.41}$$

for $k = 1, \ldots, n$

$$\alpha_k = \frac{1}{\langle Ap_k, Ap_k \rangle} \tag{2.42}$$

$$x_{k+1} = x_k + \alpha_k p_k \tag{2.43}$$

$$r_{k+1} = r_k - \alpha_k A p_k \tag{2.44}$$

$$\beta_k = \frac{1}{\langle A^a r_{k+1}, A^a r_{k+1} \rangle} \tag{2.45}$$

$$p_{k+1} = p_k + \beta_k A^a r_{k+1} \tag{2.46}$$

The algorithm is terminated at $k = n$ or when

$$\frac{||r_{k+1}||_2}{||y||_2} < \text{tolerance.} \tag{2.47}$$

In this case the magnitude of the residual will decrease at each step since it represents the actual function being minimized. Excluding the initialization, this algorithm requires two matrix vector products per iteration. The number of multiplications and divisions per iteration is $2n^2 + 5n + 2$.

Typical operator equations

The most common operators will be of integral or differential type, or a matrix derived from one or the other. If the operator A is composed of Fredholm equations of the second kind

$$\xi_1 f_x(x,y) + \iint_s [f_x(x',y')\psi_1(x,x',y,y') + f_y(x',y')\psi_2(x,x',y,y')]\, ds' = h_x(x,y) \tag{2.48}$$

$$\xi_2 f_y(x,y) + \iint_s [f_x(x',y')\psi_3(x,x',y,y') + f_y(x',y')\psi_4(x,x',y,y')]\, ds' = h_y(x,y) \tag{2.49}$$

then the adjoint operator $A^a f$ would be defined by the relations

$$\xi_1^* f_x(x,y) + \iint_s [f_x(x',y')\psi_1^*(x',x,y'y) + f_y(x',y')\psi_2^*(x',x,y'y)]\, ds' = h_x(x,y) \tag{2.50}$$

$$\xi_2^* f_y(x,y) + \iint_s [f_x(x',y')\psi_3^*(x',x,y',y) + f_y(x',y')\psi_4^*(x',x,y',y)]\, ds' = h_y(x,y). \tag{2.51}$$

If the operator A is composed of first and second order differential operators

$$\left[\frac{\partial^2}{\partial x^2} + \xi_1 \frac{\partial}{\partial x}\right] f_x(x,y) + \frac{\partial^2}{\partial x \partial y} f_y(x,y) = h_x(x,y) \tag{2.52}$$

$$\frac{\partial^2}{\partial x \partial y} f_x(x,y) + \left[\frac{\partial^2}{\partial y^2} + \xi_2 \frac{\partial}{\partial y}\right] f_y(x,y) = h_y(x,y) \tag{2.53}$$

then the adjoint operator $A^a f$ would be defined by the relations

$$\left[\frac{\partial^2}{\partial x^2} - \xi_1^* \frac{\partial}{\partial x}\right] f_x(x,y) + \frac{\partial^2}{\partial x \partial y} f_y(x,y) = h_x(x,y) \tag{2.54}$$

$$\frac{\partial^2}{\partial x \partial y} f_x(x,y) + \left[\frac{\partial^2}{\partial y^2} - \xi_2^* \frac{\partial}{\partial y}\right] f_y(x,y) = h_y(x,y). \tag{2.55}$$

If the operator A is a general complex $n \times n$ matrix then the adjoint is the complex conjugate of the transpose defined by

$$A^a = (A^T)^*. \tag{2.56}$$

CHAPTER III

DERIVATION AND COMPUTATION OF A DISCRETE FOURIER TRANSFORM USING HIGHER ORDER INTEGRATION AND PRIME FACTORIZATION

3.1 Introduction

The discrete Fourier transform (DFT) has been studied extensively by mathematicians, engineers and scientists for many years. The bibliography by Heideman et al [12] contains over 2000 reference papers concerning computation and application of the DFT. Most of the work has been concerned with increasing the speed of the computation. The purpose of this study is to develop a algorithm which is not only fast but also more accurate.

3.2 Derivation of a DFT

The DFT and inverse DFT are approximate representations of the continuous transform pair

$$\tilde{z}(f) = \int_{-\infty}^{\infty} z(x) e^{-j2\pi fx} dx \tag{3.1}$$

$$z(x) = \int_{-\infty}^{\infty} \tilde{z}(f) e^{j2\pi fx} df. \tag{3.2}$$

The transform pair is assumed to be valid. The interested reader may consult Champeney [14] for a discussion of the sufficient and necessary conditions for transformability. Assume that $z(x)$ is a complex function of bounded support such that

$$z(x) = \begin{cases} z_r(x) + jz_i(x) & \text{for } x_{min} \leq x \leq x_{max} \\ 0 & \text{otherwise.} \end{cases} \tag{3.3}$$

Under this restriction it may be shown that there exists f_{min}, f_{max} and δ such that $|\tilde{z}(f)| < \delta$ for $f \geq f_{max}$ and $f \leq f_{min}$. In a more practical sense $\tilde{z}(f)$ may be defined by

$$\tilde{z}(f) = \begin{cases} \tilde{z}_r(f) + j\tilde{z}_i(f) & \text{for } f_{min} \leq f \leq f_{max} \\ 0 & \text{otherwise.} \end{cases} \tag{3.4}$$

Let the spatial and spectral domains be segmented into N uniform cells of widths

$$\Delta x = \frac{x_{max} - x_{min}}{N} \tag{3.5}$$

$$\Delta f = \frac{f_{max} - f_{min}}{N} \tag{3.6}$$

Since the sample points are equally spaced, the cell width Δx implies a resolution limit on $|f_{max} - f_{min}|$ and Δf implies a resolution limit on $|x_{max} - x_{min}|$. These limits may be found by finding the lowest order interpolation sinusoid which passes through all the sample points.

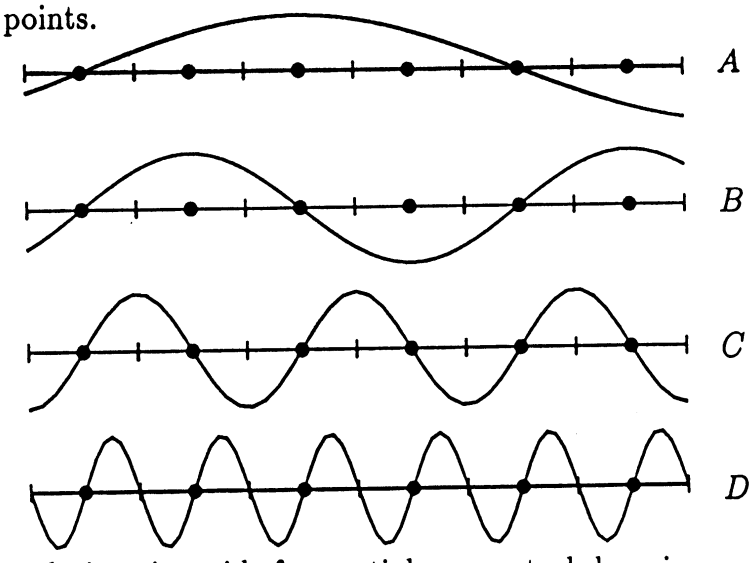

Figure 3.1. Interpolation sinusoids for spatial or spectral domain.

Observation of figure 3.1 indicates that for curves A, B, and C there is no ambiguity in terms of differenciating each curve given the set of sample values. However, curves C and D are indistinguishible based on the sample values and furthermore, there exist an infinite number of higher order interpolation sinusoids which pass through all the sample points. Curve C denotes the highest order interpolation sinusoid which may be distinguished from any other lower order sinusoid. The resolution limits are then determined by the spatial or spectral frequency of curve C as

$$f_{max} - f_{min} = \frac{1}{\Delta x} \tag{3.7}$$

$$x_{max} - x_{min} = \frac{1}{\Delta f}. \tag{3.8}$$

which combined with (3.5) and (3.6) may be used to define a quantity called the space-bandwidth product defined by

$$\Delta x \Delta f = \frac{1}{N}. \tag{3.9}$$

Note that the spatial sample interval Δx and the spectral sample interval Δf are dependent in a reciprocal manner. This is undesirable since the error in the forward and inverse Fourier transforms will be dependent on Δx and Δf respectively. Assume that the error in the forward and inverse DFT is considered minimial if $\Delta x \leq \delta_1$ and $\Delta f \leq \delta_2$ Making Δx smaller will increase N and make the forward Fourier transform more accurate but Δf remains constant. In order to increase the accuracy of the inverse Fourier transform, extra cells must be appended in the spatial domain in order to increase N without decreasing Δx. This is commonly refered to as 'padding' and in general if the number of non-zero samples is M then the total length N of the data set should satisfy $N \geq 2M$.

It is convienient to make the integration formula independent of the location of the spatial data along the x axis so making the change of variables $x = u + x_0$

and defining the quantities

$$s(u) = z(u + x_0) \tag{3.10}$$

$$\tilde{s}(f) = \tilde{z}(f)e^{j2\pi f x_0} \tag{3.11}$$

allows the transform integrals to be written as

$$\tilde{s}(f) = \int_{u_{min}}^{u_{max}} s(u)e^{-j2\pi uf}du \tag{3.12}$$

$$s(u) = \int_{f_{min}}^{f_{max}} \tilde{s}(f)e^{j2\pi uf}df = \left[\int_{f_{min}}^{f_{max}} \tilde{s}^*(f)e^{-j2\pi uf}df\right]^* \tag{3.13}$$

Assuming an even number of cells the spatial domain may be segmented as where the variables are discretized as

$$u_p = p\Delta u \qquad p = 0, ..., N-1 \tag{3.14}$$

$$f_v = v\Delta f \qquad v = -\frac{N}{2} + 1, ...\frac{N}{2} \tag{3.15}$$

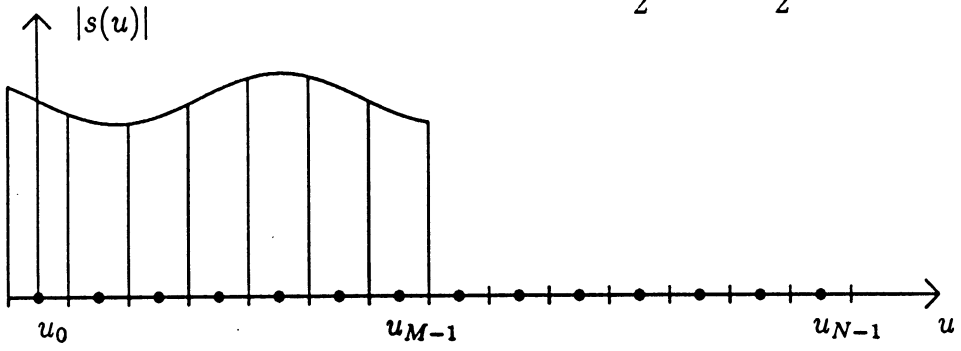

Figure 3.2. Space limited function with N cells

and similiarly, the spectral domain may be segmented as

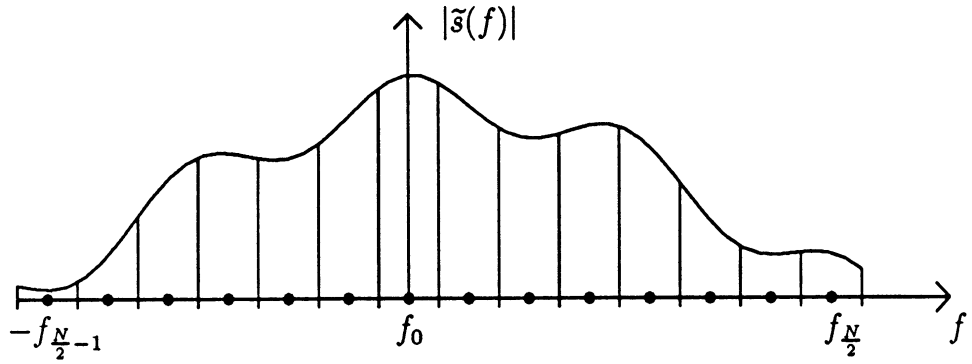

Figure 3.3. Band limited function with N cells

The integrals are approximated using an open quadrature rule of the form

$$\int_{u_{min}}^{u_{max}} s(u)e^{-j2\pi fu}du = \tilde{s}(v) = \sum_{p=0}^{N-1} s(p)\alpha_p(v)W^{pv} \tag{3.16}$$

$$\left[\int_{f_{min}}^{f_{max}} \tilde{s}^*(f)e^{-j2\pi fu}df\right]^* = s(p) = \left[\sum_{v=-\frac{N}{2}+1}^{\frac{N}{2}} \tilde{s}^*(v)\beta_v(p)W^{pv}\right]^* \tag{3.17}$$

where $W = e^{-j\frac{2\pi}{N}}$. If the indices of the sequences in (3.18) and (3.19) are interpreted as storage locations the vectors s and $\tilde{s}$ would appear in memory as

$$\begin{array}{cccccccccc} & & & & & s(0) & s(1) & s(2) & \ldots & s(\frac{N}{2}) \quad \ldots \quad s(N-1) \\ \tilde{s}(\frac{2-N}{2}) & \ldots & \tilde{s}(-2) & \tilde{s}(-1) & \tilde{s}(0) & \tilde{s}(1) & \tilde{s}(2) & \ldots & \tilde{s}(\frac{N}{2}) & \end{array} \tag{3.18}$$

In order to directly overwrite s onto $\tilde{s}$ the negative index $\tilde{s}$ elements may be shifted N elements to the right which yields

$$\begin{array}{cccccccc} s(0) & s(1) & s(2) & \ldots & s(\frac{N}{2}) & s(\frac{N}{2}+1) & \ldots & s(N-1) \\ \tilde{s}(0) & \tilde{s}(1) & \tilde{s}(2) & \ldots & \tilde{s}(\frac{N}{2}) & \tilde{s}(-\frac{N}{2}+1) & \ldots & \tilde{s}(-1) \end{array} \tag{3.19}$$

This shift has no effect on the complex exponential since $W^{p(q-N)} = W^{pq}$. A generalized non-reciprocal DFT pair may then be defined by

$$\tilde{s}_n(q) = \sum_{p=0}^{N-1} s_n(p)\alpha_p(q)W^{pq} \tag{3.20}$$

$$s(p) = \left[\sum_{q=0}^{N-1} \tilde{s}_n^*(q)\beta_q(p)W^{pq}\right]^* \tag{3.21}$$

If midpoint integration is used, $\alpha_p(q) = \Delta x$ and $\beta_p(q) = \Delta f$ yielding the conventional reciprocal DFT pair

$$\tilde{s}(q) = \sum_{p=0}^{N-1} s(p)W^{pq} \tag{3.22}$$

$$s(p) = \frac{1}{N}\left[\sum_{q=0}^{N-1} \tilde{s}^*(q)W^{pq}\right]^* \tag{3.23}$$

Although the forward and inverse transform may be generalized as above, in many cases it is sufficient to generalize only the forward transform. A common illustration of this is the evaluation of a convolution. The inverse transform of a convolution will in many cases be much smoother than any of its functional components. transformed

3.3 Higher Order Integration

The midpoint integration used to derive the conventional DFT pair implies that the entire integrand is constant over each cell. However, the cell width is chosen based on the function to be transformed not the integrand in the transform. Even if the function is constant over the cell width, the product of the function and the complex exponential becomes quite oscillatory with increasing frequency. Midpoint integration applied to a single cell yields

$$\int_{-\frac{h}{2}}^{\frac{h}{2}} z(x)e^{-j2\pi fx}dx \approx hz(x_0)e^{-j2\pi fx_0}. \tag{3.24}$$

The assumption on the integrand is that over the cell

$$[z_r(x) + jz_i(x)]e^{-j2\pi fx} = z_{r0} + jz_{i0} = \text{constant}. \tag{3.25}$$

The system of equations

$$z_r(x)\cos(2\pi fx) - z_i(x)\sin(2\pi fx) = z_{r0} \tag{3.26}$$

$$z_r(x)\sin(2\pi fx) - z_i(x)\cos(2\pi fx) = -z_{i0} \tag{3.27}$$

may be formed and solved for the unknown real and imaginary parts of $z(x)$ as

$$z_r(x) = z_{r0}\cos(2\pi fx) - z_{i0}\sin(2\pi fx) \tag{3.28}$$

$$z_r(x) = z_{r0}\sin(2\pi fx) + z_{i0}\cos(2\pi fx). \tag{3.29}$$

As these equations indicate, the implied basis functions are dependent on the frequency. Thus, the approximation that the integrand is constant becomes less valid as the frequency increases. To illustrate this, let $h = \frac{1}{20}$ such that $f_{max} = \frac{1}{2h} = 10$ and $z = 1.0 + j1.0$.

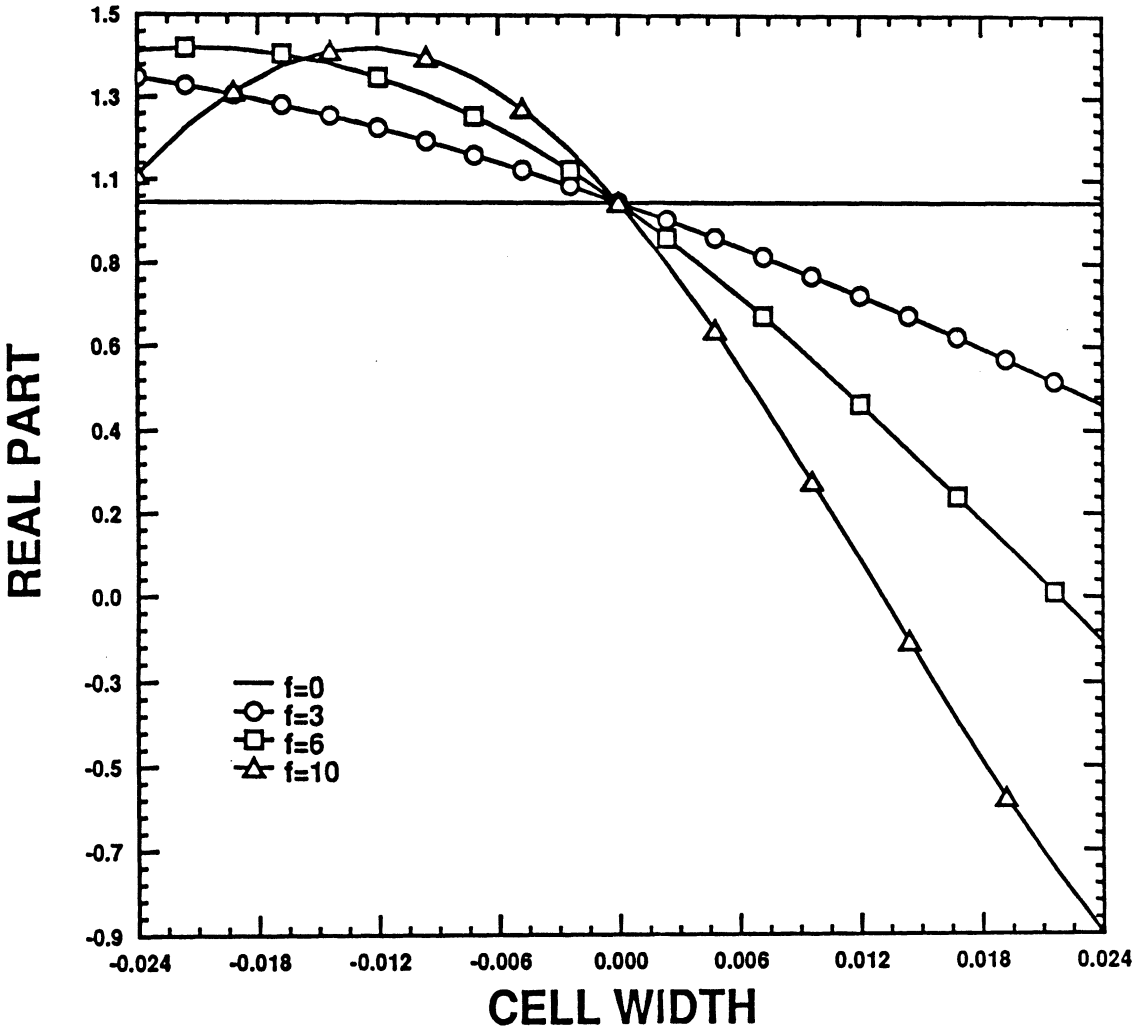

Figure 3.4. Real part of $z(x)$ assumed at each f.

3.3.1 Weighted Open Newton-Coates Integration

The simple integration used to obtain (3.24) and (3.25) does not exploit the fact that part of the integrand of (3.12) and (3.13) is known. The following formulas were derived in a manner analogous to the open Newton-Coats forms[15]. The formulas are derived for equally spaced nodes and are of the weighted open Newton-Coates (WONC) type. The weights are complex functions of f defined as $\alpha(f) = \alpha^r(f) + j\alpha^i(f)$. The nodes are defined by

$$x_k = x_0 + kh \quad k = 0, ..., n-1 \tag{3.30}$$

where

$$x_0 = a + \frac{1}{2}h \tag{3.31}$$

where

$$\alpha_n(f) = e^{2\pi f u_n} \int_a^b L_n(u) e^{-j2\pi f u} du \tag{3.32}$$

and $L_n(t)$ denotes the Lagrange polynomials defined by

$$L_n(t) = \prod_{\substack{i=0 \\ i \neq n}}^{N-1} \frac{(t - t_i)}{(t_n - t)}. \tag{3.33}$$

This study will consider the 1 and 3 point formulas. Making the definition $\psi = \pi f h$, the 1 point formula is given as

$$\int_a^b z(x) e^{-j2\pi f x} dx = \alpha_1(\psi) z(x_0) e^{-j2\pi f x_0} \tag{3.34}$$

where

$$\alpha_1^r(\psi) = h \frac{\sin(\psi)}{\psi}. \tag{3.35}$$

The composite 1 point rule is given by

$$\int_a^b z(x) e^{-j2\pi f x} dx = \alpha_1(\psi) \sum_{k=0}^{N-1} z(x_k) e^{-j2\pi f x_k} \tag{3.36}$$

and the 3 point formula yields

$$\int_a^b z(x)e^{-j2\pi fx}dx = \alpha_1(\psi)z(x_0)e^{-j2\pi fx_0} + \alpha_2(\psi)z(x_1)e^{-j2\pi fx_1} + \alpha_3(\psi)z(x_2)e^{-j2\pi fx_2} \tag{3.37}$$

where

$$\alpha_1^r(\psi) = \frac{h}{16\psi^3}\left[(3\psi^2-2)\sin(5\psi) + (15\psi^2-2)\sin(\psi) + 4\psi(\cos(5\psi)+2\cos(\psi))\right] \tag{3.38}$$

$$\alpha_1^i(\psi) = \frac{h}{16\psi^3}\left[(3\psi^2-2)\cos(5\psi) - (15\psi^2-2)\cos(\psi) - 4\psi(\sin(5\psi)-2\sin(\psi))\right] \tag{3.39}$$

$$\alpha_2(\psi) = \frac{h}{4\psi^3}\left[(2-5\psi^2)\sin(3\psi) - 6\psi\cos(3\psi)\right] \tag{3.40}$$

$$\alpha_3(\psi) = \alpha_1^*(f) \tag{3.41}$$

The composite 3 point rule may be written as

$$\begin{aligned}\int_a^b z(x)e^{-j2\pi fx}dx = {} & \alpha_1(\psi)\sum_{k=0}^{\frac{N}{3}-1} z(x_{3k})e^{-j2\pi fx_{3k}} + \alpha_2(\psi)e^{-j2\pi fh}\sum_{k=0}^{\frac{N}{3}-1} z(x_{3k+1})e^{-j2\pi fx_{3k}} \\ & + \alpha_3(\psi)e^{-j4\pi fh}\sum_{k=0}^{\frac{N}{3}-1} z(x_{3k+2})e^{-j2\pi fx_{3k}}\end{aligned} \tag{3.42}$$

3.3.2 Weighted Open Finite Difference Integration

It is possible to derive integration formulas which use not only function values but also derivative values [16]. The derivatives may then be approximated using finite differences. This integration formula will be referred to as a weighted open finite difference (WOFD) type.

$$\int_a^b s(x)e^{-j2\pi fx}dx = \left[\alpha_0 s(x_0) + \alpha_1 s'(x_0) + \alpha_2 s''(x_0)\right]e^{-j2\pi fx_0} \tag{3.43}$$

where $h = b - a$ and $x_0 = \frac{h}{2}$. The coefficients may be calculated by requiring the formula to be exact for polynomials up to and including x^n for $n = 0, ..., 2$. Thus,

this formula has the same order as the 3-pt WONC formula. An alternative and easier derivation of the coefficents is to integrate the interpolating polynomial over the interval. An interpolation scheme which uses both function and derivative values is called Birkoff interpolation. The single point integration formula is a special case of Birkoff interpolation which expands the unknown function in a Taylor polynomial around each point.

$$s(x) = s(x_0) + (x - x_0)s'(x_0) + \frac{1}{2}(x - x_0)^2 s''(x_0) \tag{3.44}$$

By inspection, the weight coefficients are expressed as the integrals

$$\alpha_0 = e^{j2\pi f x_0} \int_a^b e^{-j2\pi f x} dx \tag{3.45}$$

$$\alpha_1 = e^{j2\pi f x_0} \int_a^b (x - x_0) e^{-j2\pi f x} dx \tag{3.46}$$

$$\alpha_2 = \frac{1}{2} e^{j2\pi f x_0} \int_a^b (x - x_0)^2 e^{-j2\pi f x} dx \tag{3.47}$$

which yield

$$\alpha_0 = h\gamma_1 \tag{3.48}$$

$$\alpha_1 = j\frac{1}{2}h^2\gamma_2 \tag{3.49}$$

$$\alpha_2 = \frac{1}{24}h^3\gamma_3 \tag{3.50}$$

where

$$\gamma_1 = \frac{\sin(\psi)}{\psi} \tag{3.51}$$

$$\gamma_2 = \frac{\psi\cos(\psi) - \sin(\psi)}{\psi^2} \tag{3.52}$$

$$\gamma_3 = 3\left[\frac{(\psi^2 - 2)\sin(\psi) + 2\psi\cos(\psi)}{\psi^3}\right] \tag{3.53}$$

Extending the single point formula to a composite formula with N points yields

$$\begin{aligned}\int_a^b s(x)e^{-j2\pi f x} dx = {} & \alpha_0 \sum_{n=0}^{N-1} s(x_n)e^{-j2\pi f x_n} + \alpha_1 \sum_{n=0}^{N-1} s'(x_n)e^{-j2\pi f x_n} \\ & + \alpha_2 \sum_{n=0}^{N-1} s''(x_n)e^{-j2\pi f x_n}.\end{aligned} \tag{3.54}$$

The derivatives may be approximated using the center difference derivative rules

$$s'(x_n) \approx \frac{1}{2h}\left[s(x_{n+1}) - s(x_{n-1})\right] \tag{3.55}$$

$$s''(x_n) \approx \frac{1}{h^2}\left[s(x_{n+1}) - 2s(x_n) + s(x_{n-1})\right]. \tag{3.56}$$

The Fourier transform of the first and second derivatives is given by

$$\begin{aligned}
\int_{-\infty}^{\infty} s'(x)e^{-j2\pi fx}dx &\approx \frac{1}{2h}\int_{-\infty}^{\infty}\left[s(x+h) - s(x-h)\right]e^{-j2\pi fx}dx \\
&= \frac{1}{2h}\left[e^{j2\pi fh} - e^{-j2\pi h}\right]\int_{-\infty}^{\infty} s(x)e^{-j2\pi fx} \\
&= j\frac{1}{h}\sin(2\pi fh)\int_{-\infty}^{\infty} s(x)e^{-j2\pi fx} \qquad (3.57) \\
\int_{-\infty}^{\infty} s''(x)e^{-j2\pi fx}dx &\approx \frac{1}{h^2}\int_{-\infty}^{\infty}\left[s(x+h) - 2s(x) + s(x-h)\right]e^{-j2\pi fx}dx \\
&= \frac{1}{2h}\left[e^{j2\pi fh} - 2 + e^{-j2\pi h}\right]\int_{-\infty}^{\infty} s(x)e^{-j2\pi fx} \\
&= -\frac{2}{h^2}[1 - \cos(2\pi fh)]\int_{-\infty}^{\infty} s(x)e^{-j2\pi fx} \qquad (3.58)
\end{aligned}$$

The integral may be written as

$$\begin{aligned}
\int_{-\infty}^{\infty} s(x)e^{-j2\pi fx}dx &= \left[\alpha_0 + j\frac{1}{h}\alpha_1\sin(2\psi) - \frac{2}{h^2}\alpha_2[1-\cos(2\psi)]\right]\sum_{n=0}^{N-1} s(x_n)e^{-j2\pi fx_n} \\
&\quad +(I_0 + I_{M-1})e^{-j2\pi x_0} \qquad (3.59)
\end{aligned}$$

where I_0 and I_{M-1} are given by

$$\begin{aligned}
I_0 &= \alpha_1\left[s'(x_{-1}) - \frac{1}{2h}[s(x_0) - s(x_{-2})]\right]e^{j2\pi fh} \\
&\quad +\alpha_1\left[s'(x_0) - \frac{1}{2h}[s(x_1) - s(x_{-1})]\right] \\
&\quad +\alpha_2\left[s''(x_{-1}) - \frac{1}{h^2}[s(x_0) - 2s(x_{-1}) + s(x_{-2})]\right]e^{j2\pi fh} \\
&\quad +\alpha_2\left[s''(x_0) - \frac{1}{h^2}[s(x_1) - 2s(x_0) + s(x_{-1})]\right] \qquad (3.60) \\
I_{M-1} &= +\alpha_1\left[s'(x_{M-1}) - \frac{1}{2h}[s(x_M) - s(x_{M-2})]\right]e^{-j2\pi f(M-1)h} \\
&\quad +\alpha_1\left[s'(x_M) - \frac{1}{2h}[s(x_{M+1}) - s(x_{M-1})]\right]e^{-j2\pi fMh} \\
&\quad +\alpha_2\left[s''(x_{M-1}) - \frac{1}{h^2}[s(x_M) - 2s(x_{M-1}) + s(x_{M-2})]\right]e^{-j2\pi f(M-1)h} \\
&\quad +\alpha_2\left[s''(x_M) - \frac{1}{h^2}[s(x_{M+1}) - 2s(x_M) + s(x_{M-1})]\right]e^{-j2\pi fMh} \qquad (3.61)
\end{aligned}$$

and represent the end point corrections which replace the midpoint difference formulas by forward and backward differences, respectively. These correction terms may be simplified to

$$\begin{aligned} I_0 &= \alpha_2 s''(x_0) + \alpha_1 s'(x_0) + \frac{1}{2h^2}\left[2\alpha_2(2 - e^{j2\psi}) - h\alpha_1 e^{j2\psi}\right] s(x_0) \\ &\quad -\frac{1}{2h^2}\left[h\alpha_1 + 2\alpha_2\right] s(x_1) \qquad (3.62) \\ I_{M-1} &= \left[\alpha_2 s''(x_{M-1}) + \alpha_1 s'(x_{M-1})\right] e^{-j2(M-1)\psi} \\ &\quad +\frac{1}{2h^2}\left[h\alpha_1 - 2\alpha_2(1 - e^{j2\psi})\right] e^{-j2M\psi} s(x_{M-1}) \\ &\quad +\frac{1}{2h^2}\left[h\alpha_1 - 2\alpha_2\right] e^{-j2(M-1)\psi} s(x_{M-2}) \qquad (3.63) \end{aligned}$$

by excluding all points outside the interval. The derivatives at the initial points may be approximated with forward difference rules

$$\begin{aligned} s'(x_0) &\approx -\frac{1}{2h}\left[s(x_2) - 4s(x_1) + 3s(x_0)\right] \qquad (3.64) \\ s''(x_0) &\approx \frac{1}{h^2}\left[s(x_2) - 2s(x_1) + s(x_0)\right]. \qquad (3.65) \end{aligned}$$

Similarily, the end point derivatives may be approximated using the backward difference rules

$$\begin{aligned} s'(x_{M-1}) &\approx \frac{1}{2h}\left[3s(x_{M-1}) - 4s(x_{M-2}) + s(x_{M-3})\right] \qquad (3.66) \\ s''(x_{M-1}) &\approx \frac{1}{h^2}\left[s(x_{M-1}) - 2s(x_{M-2}) + s(x_{M-3})\right]. \qquad (3.67) \end{aligned}$$

Making the assumption that $s(x_n) = 0$ for $n > M - 1$ (3.59) may be rewritten as

$$\begin{aligned} \int_{-\infty}^{\infty} s(x) e^{-j2\pi f x} dx &= \zeta_1 \sum_{n=0}^{N-1} s(x_n) e^{-j2\pi f x_n} \\ &\quad + \left[\zeta_2 s(x_0) + \zeta_3 s(x_1) + \zeta_4 s(x_2)\right] e^{-j2\pi x_0} \\ &\quad + \left[\zeta_5 s(x_{M-1}) + \zeta_6 s(x_{M-2}) + \zeta_7 s(x_{M-3})\right] e^{-j2\pi x_0} \qquad (3.68) \end{aligned}$$

where, letting $\theta = M\psi$

$$\zeta_1 = h\left[\gamma_1 - \frac{1}{2}\gamma_2 \sin(2\psi) - \frac{1}{12}\gamma_3[1 - \cos(2\psi)]\right] \qquad (3.69)$$

$$\zeta_2 = \frac{h}{24}[6\gamma_2 \sin(2\psi) + \gamma_3[3 - \cos(2\psi)]]$$
$$-j\frac{h}{24}[6\gamma_2[3 + \cos(2\psi)] + \gamma_3 \sin(2\psi)] \quad (3.70)$$

$$\zeta_3 = -\frac{h}{8}[\gamma_3 - j6\gamma_2] \quad (3.71)$$

$$\zeta_4 = \frac{h}{24}[\gamma_3 - j6\gamma_2] \quad (3.72)$$

$$\zeta_5 = \frac{h}{24}[6[3\sin(2(\theta-\psi)) + \sin(2\theta)]\gamma_2 + [3\cos(2(\theta-\psi)) - \cos(2\theta)]\gamma_3]$$
$$+j\frac{h}{24}[6[3\cos(2(\theta-\psi)) + \cos(2\theta)]\gamma_2 - [3\sin(2(\theta-\psi)) - \sin(2\theta)]\gamma_3] \quad (3.73)$$

$$\zeta_6 = -\frac{h}{8}[3\gamma_2 \sin(2(\theta-\psi)) + \gamma_3 \cos(2(\theta-\psi))$$
$$+j[3\gamma_2 \cos(2(\theta-\psi)) - \gamma_3 \sin(2(\theta-\psi))]] \quad (3.74)$$

$$\zeta_7 = \frac{h}{24}[6\gamma_2 \sin(2(\theta-\psi)) + \gamma_3 \cos(2(\theta-\psi))$$
$$+j[6\gamma_2 \cos(2(\theta-\psi)) - \gamma_3 \sin(2(\theta-\psi))]]. \quad (3.75)$$

3.3.3 Operation Count

Table 3.1 shows the operation count comparison for the conventional FFT verses the 1pt and 3pt WONC formulas and the 2nd order 1pt WOFD formula.

Type	real mult.	real add.
FFT	$c_1 N$	$c_2 N$
1pt (WONC)	$c_1 N + 2N$	$c_2 N$
3pt (WONC)	$3c_1 N + 6N$	$c_2 N + 2N$
1pt (WOFD)	$c_1 N + 24N$	$c_2 N + 14N$

Table 3.1. Operation count

As the next section will show for $60 < N < 504$ the constants c_1 and c_2 approximately range over $3 < c_1 < 5$ and $18 < c_2 < 27$. For functions with

sharp end point discontinuities the 3pt WONC formula would be more efficient. However, if the function approches zero in a smooth manner at the end points, then the end point corrections of the 1pt WOFD may be neglected and it becomes as efficient as the 1pt WONC.

3.4 Derivation of a Prime Factor FFT

The FFT is a fast method of computing a summation of the form

$$\tilde{z}(q) = \sum_{p=0}^{N-1} z(p)W^{pq}. \tag{3.76}$$

where $W = e^{-j\frac{2\pi}{N}}$ and $N = N_1N_2N_3\cdots N_m$. The basic strategy of computation is to map each one-dimensional index p and q onto a N-dimensional map which allows the summation to be accomplished in a more efficient manner. W^{pq} may be factored as

$$W^{pq} = W_1^{p_1q_1}W_2^{p_2q_2}W_3^{p_3q_3}\cdots W_m^{p_mq_m} \tag{3.77}$$

and the single summation becomes a nested set of m N_k point summations

$$\tilde{z}(q) = \sum_{p_m=0}^{N_m-1}\cdots\sum_{p_3=0}^{N_3-1}\left[\sum_{p_2=0}^{N_2-1}\left[\sum_{p_1=0}^{N_1-1} z(p)W_1^{p_1q_1}\right]W_2^{p_2q_2}\right]W_3^{p_3q_3}\cdots W_m^{p_mq_m} \tag{3.78}$$

where $W_k = W^{\frac{N}{N_k}}$. The indices p and q are refered as the input and output maps respectively. One possible mapping would be to let each factor N_k represent the base of a number system and express the input and output maps in mixed radix notation. This mapping attributed to Cooley and Tukey [17] expresses p and q as

$$\begin{aligned} p &= p_m + N_mp_{m-1} + N_{m-1}N_mp_{m-2} + N_{m-2}N_{m-1}N_mp_{m-3} + \ldots + N_2\cdots N_mp_1 \\ q &= q_1 + N_1q_2 + N_1N_2q_3 + \ldots + N_1\cdots N_{m-1}q_m \end{aligned} \tag{3.79}$$

Note that the order of the radix expression for the output map is the reverse of the input map. Performing the multiplication pq yields

$$pq = \frac{N}{N_1}p_1q_1 + \frac{N}{N_2}p_2q_2 + \frac{N}{N_3}p_3q_3\cdots\frac{N}{N_m}p_mq_m + nN^2p_uq_v + \alpha p_rq_s \tag{3.80}$$

where n is an integer, α is real and $u \neq v$, $r \neq s$. The first m terms of (3.96) represent m N_k point DFT's. The next term may be ignored since $W^{nN^2 p_u q_v} = 1$ for all n, p, q. The last term represents the cross product terms which are the 'twiddle factors' in [18]. It is possible to avoid these twiddle factors by using a different map construction.

An understanding of the prime factor algorithm requires a few introductory terms from number theory. A congruence relation is defined by assuming that a is congruent to b Modulo N if a and b yield the same remainder when divided by N. A congruence is defined by

$$a \equiv b \pmod{N} \tag{3.81}$$

A set integers is called mutually prime if the greatest common divisor between them is 1. The prime factor mapping is based on the following theorem. The Chinese Remainder Theorem [19] states that given a set of mutually prime integers $\{N_1, N_2, N_3, ..., N_m\}$ the system of congruences

$$x \equiv r_k \pmod{N} \quad k = 1, ..., m \tag{3.82}$$

has a unique solution $x \pmod{N}$. Two basic maps were suggested by Goode [20] and called the Sino and Ruritanian maps, respectively. Both of these expansions use the same map for input and output. The Sino map may be constructed as follows. Let

$$p = L_1 \frac{N}{N_1} p_1 + L_2 \frac{N}{N_2} p_2 + L_3 \frac{N}{N_3} p_3 + ... + L_m \frac{N}{N_m} p_m \pmod{N} \tag{3.83}$$

$$q = L_1 \frac{N}{N_1} q_1 + L_2 \frac{N}{N_2} q_2 + L_3 \frac{N}{N_3} p_3 + ... + L_m \frac{N}{N_m} q_m \pmod{N} \tag{3.84}$$

then there is a one to one correspondence between p and $\{p_1, p_2, p_3, ..., p_m\}$ and between q and $\{q_1, q_2, q_3, ..., q_m\}$ if the integers $L_1, L_2, L_3, ..., L_m$ are chosen such that

$$L_k \frac{N}{N_k} \equiv 1 \pmod{N_k} \quad k = 1, ..., m \tag{3.85}$$

Unfortunately, a numerical implementation of the DFT using this map will either require the solution of this set of congruences for each N or require auxillary storage of a precomputed set. This is somewhat undersirable since speed is of prime importance. An alternative called the Ruritanian map is a special case of the Sino map where $L_k = 1$ for $k = 1, ..., m$.

$$p = \frac{N}{N_1}p_1 + \frac{N}{N_2}p_2 + \frac{N}{N_3}p_3 + ... + \frac{N}{N_m}p_m \pmod{N} \tag{3.86}$$

$$q = \frac{N}{N_1}q_1 + \frac{N}{N_2}q_2 + \frac{N}{N_3}p_3 + ... + \frac{N}{N_m}q_m \pmod{N} \tag{3.87}$$

Since W is periodic in N $W^{\langle u \rangle_N \langle v \rangle_N} = W^{uv}$ and the exponent does not have to be evaluated Module N. Performing the multiplication pq yields

$$pq = \frac{N^2}{N_1^2}p_1q_1 + \frac{N^2}{N_2^2}p_2q_2 + \frac{N^2}{N_3^2}p_3q_3 + ...\frac{N^2}{N_m^2}p_mq_m + nN^2 \tag{3.88}$$

where n is an integer. W^{pq} may now be factored as

$$W^{pq} = (W_1^{p_1q_1})^{\frac{N}{N_1}}(W_2^{p_2q_2})^{\frac{N}{N_2}}(W_3^{p_3q_3})^{\frac{N}{N_3}} \cdots (W_m^{p_mq_m})^{\frac{N}{N_m}}. \tag{3.89}$$

This factorization is not in the desired form because each $W_k^{p_kq_k}$ is raised to the power $\frac{N}{N_k}$. However, it may be shown [21]-[23] that if $\frac{N}{N_k}$ is mutually prime to N_k the effect of the exponent is to permute the output N_k point sequence. Replace the output sequence

$$s(n_i) \qquad i = 0, ...k-1 \tag{3.90}$$

by the permuted sequence

$$s(n_r) \qquad r = i\frac{N}{N_k} \pmod{N_k} \text{ for } i = 0, ...k-1 \tag{3.91}$$

It is not apparent which way to sequence through the indices. As an example consider $N = 2 \cdot 3 \cdot 5 = 30$. The index sequences are given in table 3.2.

stage 1				stage 2				stage 3			
p_1	p_2	p_3	p	p_1	p_2	p_3	p	p_1	p_2	p_3	p
0	0	0	1	0	0	0	1	0	0	0	1
1	0	0	16	0	1	0	11	0	0	1	7
0	1	1	17	0	2	0	21	0	0	2	13
1	1	1	2	1	0	1	22	0	0	3	19
0	2	2	3	1	1	1	2	0	0	4	25
1	2	2	18	1	2	1	12	1	1	0	26
0	0	3	19	0	0	2	13	1	1	1	2
1	0	3	4	0	1	2	23	1	1	2	8
0	1	4	5	0	2	2	3	1	1	3	14
1	1	4	20	1	0	3	4	1	1	4	20
0	2	0	21	1	1	3	14	0	2	0	21
1	2	0	6	1	2	3	24	0	2	1	27
0	0	1	7	0	0	4	25	0	2	2	3
1	0	1	22	0	1	4	5	0	2	3	9
0	1	2	23	0	2	4	15	0	2	4	15
1	1	2	8	1	0	0	16	1	0	0	16
0	2	3	9	1	1	0	26	1	0	1	22
1	2	3	24	1	2	0	6	1	0	2	28
0	0	4	25	0	0	1	7	1	0	3	4
1	0	4	10	0	1	1	17	1	0	4	10
0	1	0	11	0	2	1	27	0	1	0	11
1	1	0	26	1	0	2	28	0	1	1	17
0	2	1	27	1	1	2	8	0	1	2	23
1	2	1	12	1	2	2	18	0	1	3	29
0	0	2	13	0	0	3	19	0	1	4	5
1	0	2	28	0	1	3	29	1	2	0	6
0	1	3	29	0	2	3	9	1	2	1	12
1	1	3	14	1	0	4	10	1	2	2	18
0	2	4	15	1	1	4	20	1	2	3	24
1	2	4	30	1	2	4	30	1	2	4	30

Table 3.2. Index sequence for $N = 2 \cdot 3 \cdot 5$.

Table 3.3 shows the possible factors for N chosen from the list of $\{2, 3, 4, 5, 7, 8, 9, 16\}$. Let

$$\alpha_k = \text{multiplications for kth factor DFT} \tag{3.92}$$

$$\beta_k = \text{additions for kth factor DFT} \tag{3.93}$$

then for $N = N_1 N_2 N_3 \cdots N_m$

$$\text{total multiplications} = \sum_{k=1}^{m} \frac{N}{N_k} \alpha_k \tag{3.94}$$

$$\text{total additions} = \sum_{k=1}^{m} \frac{N}{N_k} \beta_k \tag{3.95}$$

N	Factors	Mult.	add.	N	Factors	Mult.	Add.
2	2	0	4	80	5 · 16	260	1284
3	3	4	12	84	3 · 4 · 7	304	1536
4	4	0	16	90	2 · 5 · 9	380	1996
5	5	10	34	105	3 · 5 · 7	590	2214
6	2 · 3	8	36	112	7 · 16	396	2188
7	7	16	72	120	3 · 5 · 8	460	2076
8	8	4	52	126	2 · 7 · 9	568	2780
9	9	20	88	140	4 · 5 · 7	600	2952
10	2 · 5	20	88	144	9 · 16	500	2740
12	3 · 4	16	96	168	3 · 7 · 8	692	3492
14	2 · 7	32	172	180	4 · 5 · 9	760	3704
15	3 · 5	50	162	210	2 · 3 · 5 · 7	1180	4848
16	16	20	148	240	3 · 5 · 16	1100	4812
18	2 · 9	40	212	252	4 · 7 · 9	1136	6064
20	4 · 5	40	216	280	5 · 7 · 8	1340	6604
21	3 · 7	76	300	315	5 · 7 · 9	2050	8462
24	3 · 8	44	252	336	3 · 7 · 16	1636	7908
28	4 · 7	64	400	360	5 · 8 · 9	1700	8308
30	2 · 3 · 5	100	384	420	3 · 4 · 5 · 7	2360	10536
35	5 · 7	150	598	504	8 · 7 · 9	2524	13388
36	4 · 9	80	496	560	5 · 7 · 16	3100	14748
40	5 · 8	100	532	630	2 · 5 · 7 · 9	4100	21964
42	2 · 3 · 7	152	684	720	5 · 9 · 16	3940	18596
45	5 · 9	190	746	840	3 · 5 · 7 · 8	5140	23172
48	3 · 16	124	636	1008	7 · 9 · 16	5804	29548
56	7 · 8	156	940	1260	4 · 5 · 7 · 9	8200	38888
60	3 · 4 · 5	200	1104	1680	3 · 5 · 7 · 16	11540	50964
63	7 · 9	284	1264	2520	5 · 7 · 8 · 9	17660	84076
70	2 · 5 · 7	300	1588	5040	5 · 7 · 9 · 16	39100	182012
72	8 · 9	196	1172				

Table 3.3. Real multiplications and additions

3.5 Extension to Two Dimensions

The two dimensional fourier transform and inverse transform are defined as

$$\tilde{z}(f_x, f_y) = \int_{-\infty}^{\infty}\int_{-\infty}^{\infty} z(x,y)e^{-j2\pi(f_x x + f_y y)}dx, dy \tag{3.96}$$

$$z(x,y) = \int_{-\infty}^{\infty}\int_{-\infty}^{\infty} \tilde{z}(f_x, f_y)e^{j2\pi(f_x x + f_y y)}df_x, df_y \tag{3.97}$$

Making the change of variables $x = u + x_0$ and $y = v + y_0$ and defining the quantities

$$s(u,v) = z(u + x_0, v + y_0) \tag{3.98}$$

$$\tilde{s}(f_x, f_y) = \tilde{z}(f_x, f_y)e^{j2\pi(f_x x_0 + f_y y_0)} \tag{3.99}$$

the transform pair may be written as

$$\tilde{s}(f_u, f_v) = \int_{-\infty}^{\infty}\int_{-\infty}^{\infty} s(u,v)e^{-j2\pi(f_u u + f_v v)}du, dv \tag{3.100}$$

$$s(u,v) = \int_{-\infty}^{\infty}\int_{-\infty}^{\infty} \tilde{s}(f_u, f_v)e^{j2\pi(f_u u + f_v v)}df_u, df_v. \tag{3.101}$$

Since the exponential kernal of the integral is separable, the two-dimensional DFT may be decomposed into a series of one-dimensional DFT's. Because the data set is padded, a significant savings in computation time may be achieved by avoiding any unnecessary one-dimensional DFT's of sets of zeros. The two-dimemsional DFT is decomposed as shown in figure 3.5.

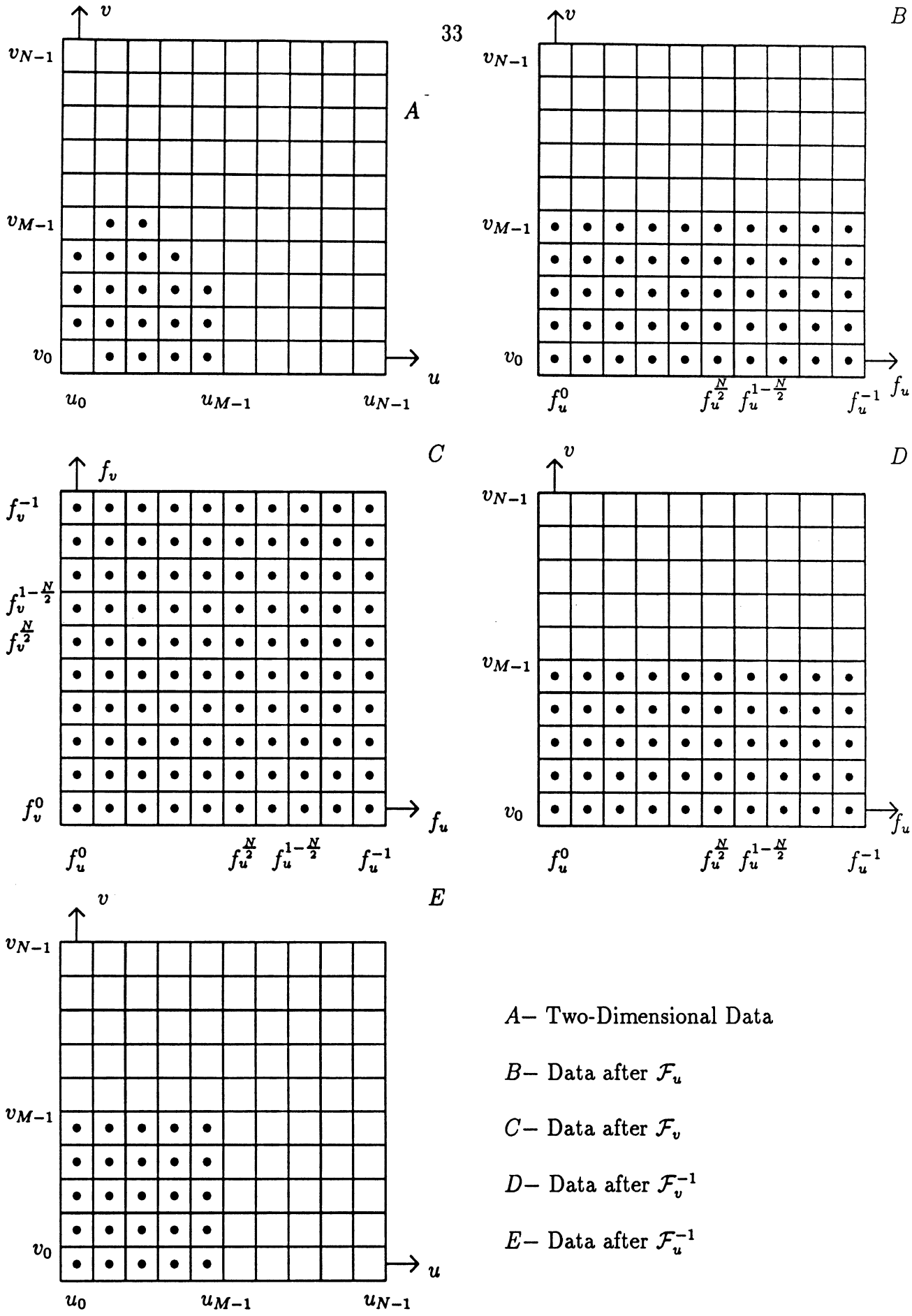

A– Two-Dimensional Data

B– Data after $\mathcal{F}_u$

C– Data after $\mathcal{F}_v$

D– Data after $\mathcal{F}_v^{-1}$

E– Data after $\mathcal{F}_u^{-1}$

Figure 3.5. Two-dimensional DFT Operations.

3.6 Test Results

The formulation was tested with a function

$$z(x) = \begin{cases} z(x) & \text{for } -a \leq x \leq a \\ 0 & \text{otherwise} \end{cases} \tag{3.102}$$

which is expanded as a finite sum of Chebyshev polynomials $T_k(\xi(x))$ where

$$z^{r,i}(x) = \sum_{k=0}^{4} c_k^{r,i} T_k(\xi(x)) \tag{3.103}$$

and $\xi(x) = \frac{x}{a}$.

Test Coefficients		
k	c_k^r	c_k^i
0	0.0	0.0
1	0.4	0.4
2	0.8	0.2
3	0.5	0.5
4	1.2	0.3

Table 3.4. Test coefficients.

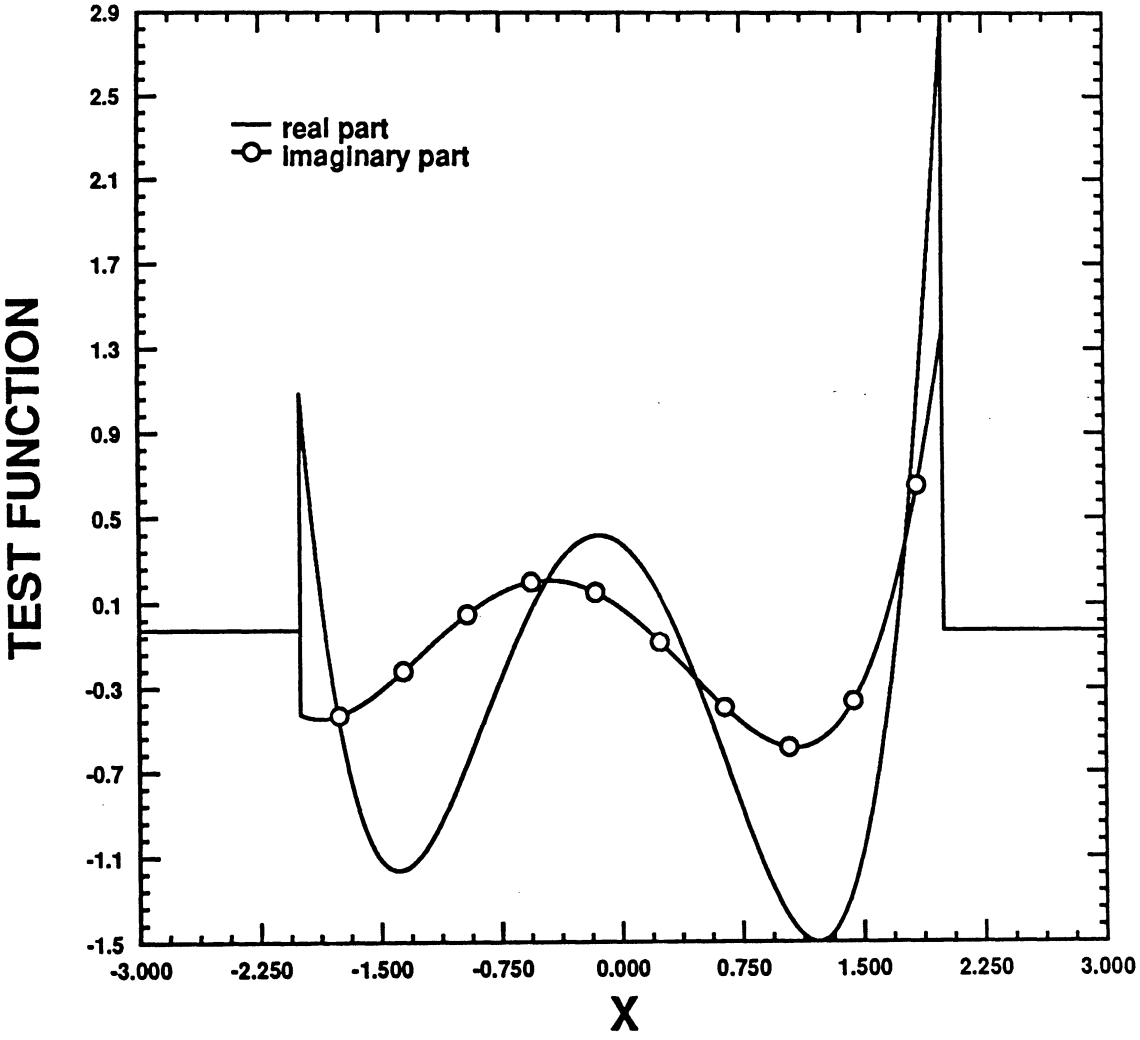

Figure 3.6. Test function.

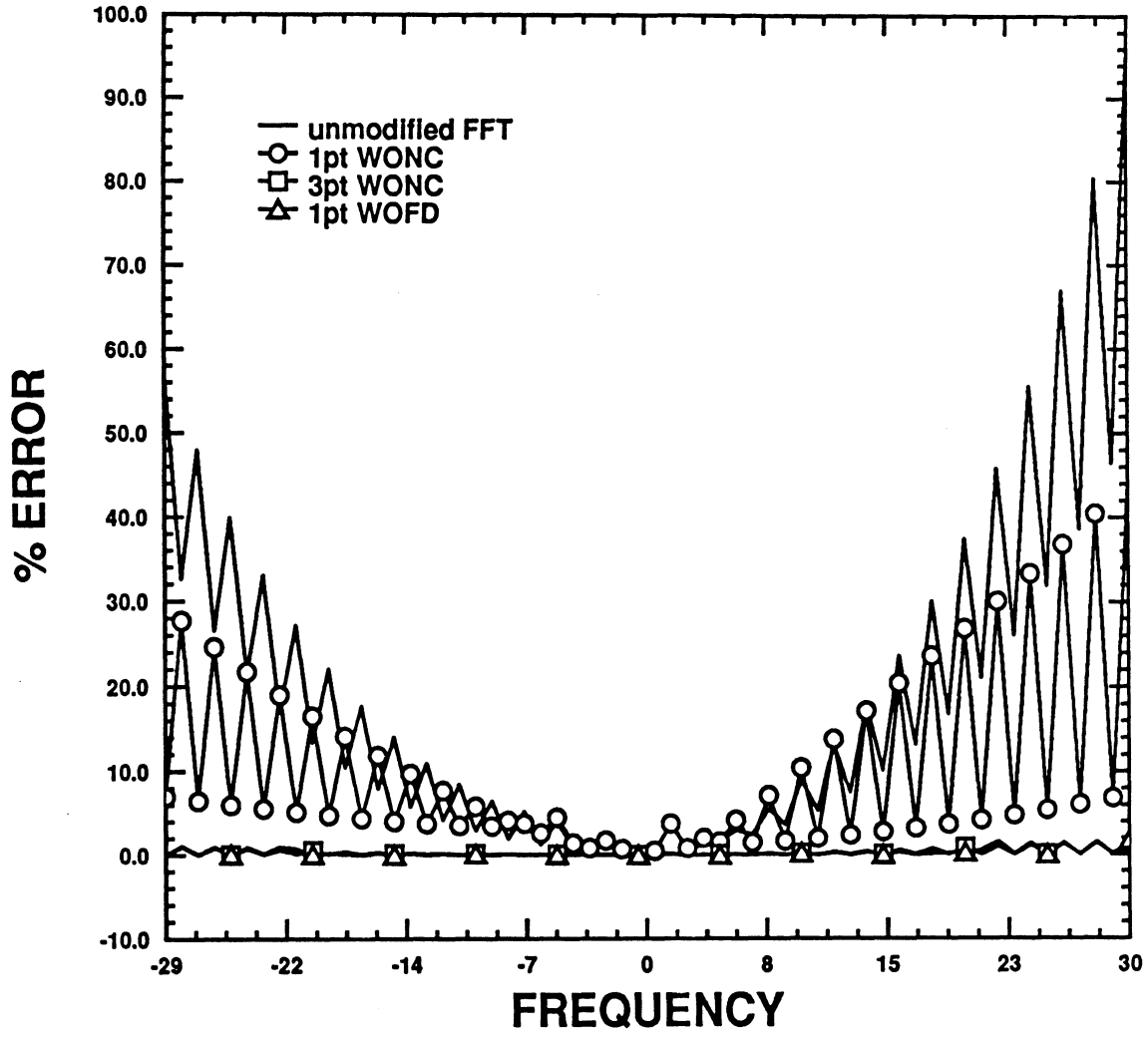

Figure 3.7. Percent error.

CHAPTER IV

SCATTERING FROM A SINGLE PLANAR PLATE

4.1 Orientation

The orientation of the plate is given as in figure 4.1.

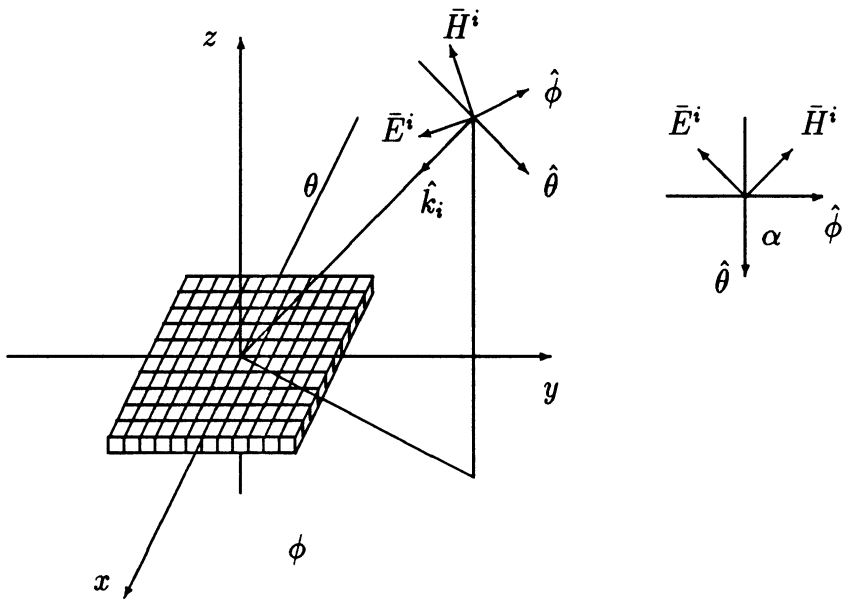

Figure 4.1. Plate with plane wave incidence.

The incident electric field has unity amplitude and may be decomposed into the orthogonal components

$$\bar{E}^i = [(\hat{\alpha}\cdot\hat{\theta})\hat{\theta} + (\hat{\alpha}\cdot\hat{\phi})\hat{\phi}]e^{-j(\bar{k}_i\cdot\bar{r})} = [E_{xo}\hat{x} + E_{yo}\hat{y} + E_{zo}\hat{z}]\,h^i \tag{4.1}$$

where

$$\bar{k}_i\cdot\bar{r} = -k_0\left[\sin(\theta_i)\cos(\phi_i)x + \sin(\theta_i)\sin(\phi_i)y\right]. \tag{4.2}$$

$$E_{xo} = \cos(\alpha_i)\cos(\theta_i)\cos(\phi_i) - \sin(\alpha_i)\sin(\phi_i) \tag{4.3}$$

$$E_{yo} = \cos(\alpha_i)\cos(\theta_i)\sin(\phi_i) + \sin(\alpha_i)\cos(\phi_i) \tag{4.4}$$

$$E_{zo} = -\cos(\alpha_i)\sin(\theta_i) \tag{4.5}$$

and $h^i = e^{-j(\bar{k}_i\cdot\bar{r})}$. The corresponding magnetic field components are computed from $\bar{H}^i = \frac{1}{Z_0}\hat{k}_i \times \bar{E}^i = [H_{xo}\hat{x} + H_{yo}\hat{y} + H_{zo}\hat{z}]h^i$ where

$$H_{xo} = \frac{1}{Z_0}[\sin(\alpha_i)\cos(\theta_i)\cos(\phi_i) + \cos(\alpha_i)\sin(\phi_i)] \tag{4.6}$$

$$H_{yo} = \frac{1}{Z_0}[\sin(\alpha_i)\cos(\theta_i)\sin(\phi_i) - \cos(\alpha_i)\cos(\phi_i)] \tag{4.7}$$

$$H_{zo} = -\frac{1}{Z_0}\sin(\alpha_i)\sin(\theta_i). \tag{4.8}$$

The E-polarization case is defined at $\alpha_i = 90°$ and H-polarization occurs at $\alpha_i = 0°$.

4.2 Integral Equations

The scattered fields may be written in terms of vector potentials as

$$\bar{E}^s = -\nabla\times\bar{F} - j\frac{Z_0}{k_0}(\nabla\times\nabla\times\bar{A} - \bar{J}^e) \tag{4.9}$$

$$\bar{H}^s = \nabla\times\bar{A} - j\frac{1}{k_0 Z_0}(\nabla\times\nabla\times\bar{F} - \bar{J}^m) \tag{4.10}$$

where $\bar{J}^{e,m}$ are electric and magnetic polarization currents and $\bar{A}$ and $\bar{F}$ satisfy the inhomogeneous vector Helmholtz equations

$$\nabla^2\bar{A} + k_0^2\bar{A} = -\bar{J}^e \tag{4.11}$$

$$\nabla^2\bar{F} + k_0^2\bar{F} = -\bar{J}^m \tag{4.12}$$

which have the solutions in integral form given by

$$\bar{A} = \iiint_{v'} \bar{J}^e(\bar{R}')G(\bar{R},\bar{R}')dv' \tag{4.13}$$

$$\bar{F} = \iiint_{v'} \bar{J}^m(\bar{R}')G(\bar{R},\bar{R}')dv' \tag{4.14}$$

with

$$G(\bar{R},\bar{R}') = \frac{e^{-jk_0|\bar{R}-\bar{R}'|}}{4\pi|\bar{R}-\bar{R}'|}. \tag{4.15}$$

The incident fields induce electric and magnetic polarization currents inside the material body. The total internal fields are expressed in terms of the currents as $E^T = \beta_e \bar{J}^e$ and $H^T = \beta_m \bar{J}^m$ where

$$\beta_e = \frac{-jZ_0}{(\epsilon_r - 1)k_0} \tag{4.16}$$

$$\beta_m = \frac{-j}{(\mu_r - 1)k_0 Z_0}. \tag{4.17}$$

These currents represent the source of the scattered field and are the solutions of the volume integral equations formed by relating the internal total, scattered and incident fields as

$$\bar{E}^T - \bar{E}^s = \bar{E}^i \tag{4.18}$$

$$\bar{H}^T - \bar{H}^s = \bar{H}^i. \tag{4.19}$$

If the plate is electrically thin, the internal field components are assumed to have a constant z variation such that $\frac{\partial}{\partial z} = 0$. It is convenient for computational purposes to express the integral equations in terms of tangential variables such that the normal components E_z and H_z are found from (4.9) and (4.10) directly and the tangential components are found after substituting (4.11) and (4.12) into (4.9) and (4.10). The volume integral equations may then be implicitly written as

$$\beta_e J_x^e + j\frac{Z_0}{k_0}\left[\left(k_0^2 + \frac{\partial^2}{\partial x^2}\right)A_x + \frac{\partial^2}{\partial x \partial y}A_y\right] + \frac{\partial}{\partial y}F_z = E_x^i \tag{4.20}$$

$$\beta_e J_y^e + j\frac{Z_0}{k_0}\left[\frac{\partial^2}{\partial x \partial y}A_x + \left(k_0^2 + \frac{\partial^2}{\partial y^2}\right)A_y\right] - \frac{\partial}{\partial x}F_z = E_y^i \tag{4.21}$$

$$\epsilon_r \beta_e J_z^e - \frac{\partial}{\partial y} F_x + \frac{\partial}{\partial x} F_y - j \frac{Z_0}{k_0} \left(\frac{\partial^2}{\partial y^2} + \frac{\partial^2}{\partial x^2} \right) A_z = E_z^i \tag{4.22}$$

$$\beta_m J_x^m + j \frac{1}{k_0 Z_0} \left[\left(k_0^2 + \frac{\partial^2}{\partial x^2} \right) F_x + \frac{\partial^2}{\partial x \partial y} F_y \right] - \frac{\partial}{\partial y} A_z = H_x^i \tag{4.23}$$

$$\beta_m J_y^m + j \frac{1}{k_0 Z_0} \left[\frac{\partial^2}{\partial x \partial y} F_x + \left(k_0^2 + \frac{\partial^2}{\partial y^2} \right) F_y \right] + \frac{\partial}{\partial x} A_z = H_y^i \tag{4.24}$$

$$\mu_r \beta_m J_z^m + \frac{\partial}{\partial y} A_x - \frac{\partial}{\partial x} A_y - j \frac{1}{k_0 Z_0} \left(\frac{\partial^2}{\partial y^2} + \frac{\partial^2}{\partial x^2} \right) F_z = H_z^i. \tag{4.25}$$

Since the volume current has no z variation, the volume integral may be reduced to a surface integral. The volume currents may then be replaced by an equivalent normalized electric surface current $\bar{K}^e = \tau \bar{J}^e Z_0^{-1}$ and a magnetic surface current $\bar{K}^m = \tau \bar{J}^m$. Assuming that the coordinates are normalized with respect to λ_0 (4.20)-(4.25) reduce to

$$w_1 K_x^e + \iint_{S'} \left[\Psi_1 K_x^e + \Psi_2 K_y^e + \Psi_6 K_z^m \right] dS' = E_x^i \tag{4.26}$$

$$w_1 K_y^e + \iint_{S'} \left[\Psi_2 K_x^e + \Psi_3 K_y^e - \Psi_5 K_z^m \right] dS' = E_y^i \tag{4.27}$$

$$w_2 K_z^e - \iint_{S'} \left[\Psi_6 K_x^m - \Psi_5 K_y^m + \Psi_4 K_z^e \right] dS' = E_z^i \tag{4.28}$$

$$w_3 K_x^m + \iint_{S'} \left[\Psi_1 K_x^m + \Psi_2 K_y^m - \Psi_6 K_z^e \right] dS' = H_x^i \tag{4.29}$$

$$w_3 K_y^m + \iint_{S'} \left[\Psi_2 K_x^m + \Psi_3 K_y^m + \Psi_5 K_z^e \right] dS' = H_y^i \tag{4.30}$$

$$w_2 K_z^m + \iint_{S'} \left[\Psi_6 K_x^e - \Psi_5 K_y^e - \Psi_4 K_z^m \right] dS' = H_z^i \tag{4.31}$$

where

$$\Psi_1 = j \frac{1}{2\pi} \left(4\pi^2 + \frac{\partial^2}{\partial x^2} \right) G \qquad \Psi_2 = j \frac{1}{2\pi} \frac{\partial^2}{\partial x \partial y} G \tag{4.32}$$

$$\Psi_3 = j \frac{1}{2\pi} \left(4\pi^2 + \frac{\partial^2}{\partial y^2} \right) G \qquad \Psi_4 = j \frac{1}{2\pi} \left(\frac{\partial^2}{\partial x^2} + \frac{\partial^2}{\partial y^2} \right) G \tag{4.33}$$

$$\Psi_5 = \frac{\partial}{\partial x} G \qquad \Psi_6 = \frac{\partial}{\partial y} G \tag{4.34}$$

and

$$w_1 = -j \frac{1}{(\epsilon_r - 1) 2\pi\tau} = \frac{1}{2\pi\tau} \left[\frac{\epsilon_r'' + j(1 - \epsilon_r')}{(\epsilon_r' - 1)^2 + (\epsilon_r'')^2} \right] \tag{4.35}$$

$$w_2 = -j \frac{\epsilon_r}{(\epsilon_r - 1) 2\pi\tau} = \frac{1}{2\pi\tau} \left[\frac{\epsilon_r'' - j[\epsilon_r'(\epsilon_r' - 1) + (\epsilon_r'')^2]}{(\epsilon_r' - 1)^2 + (\epsilon_r'')^2} \right] \tag{4.36}$$

$$w_3 = -j\frac{1}{(\mu_r-1)2\pi\tau} = \frac{1}{2\pi\tau}\left[\frac{\mu_r''+j(1-\mu_r')}{(\mu_r'-1)^2+(\mu_r'')^2}\right] \tag{4.37}$$

$$w_4 = -j\frac{\mu_r}{(\mu_r-1)2\pi\tau} = \frac{1}{2\pi\tau}\left[\frac{\mu_r''-j[\mu_r'(\mu_r'-1)+(\mu_r'')^2]}{(\mu_r'-1)^2+(\mu_r'')^2}\right] \tag{4.38}$$

The two dimensional fourier transform and inverse transform are defined as

$$\tilde{g}(f_x,f_y) = \int_{-\infty}^{\infty}\int_{-\infty}^{\infty} g(x,y)e^{-j2\pi(f_x x+f_y y)}dx,dy \tag{4.39}$$

$$g(x,y) = \int_{-\infty}^{\infty}\int_{-\infty}^{\infty} \tilde{g}(f_x,f_y)e^{j2\pi(f_x x+f_y y)}df_x,df_y. \tag{4.40}$$

The two dimensional green's function has a fourier transform given by

$$\frac{e^{-j2\pi\sqrt{x^2+y^2}}}{4\pi\sqrt{x^2+y^2}} \longleftrightarrow \begin{cases} -j\frac{d}{2\pi} & \text{for } f_x^2+f_y^2<1 \\ \frac{d}{2\pi} & \text{for } f_x^2+f_y^2>1 \end{cases} \tag{4.41}$$

where $d=\frac{1}{2}(|f_x^2+f_y^2-1|)^{-\frac{1}{2}}$. Let $\widetilde{X}$ denote the fourier transform and X^* signify complex conjugation. The fourier transforms of (4.32)-(4.34) are

$$\tilde{\Psi}_{1r} = \begin{cases} \tilde{\zeta}_1 & \text{for } f_x^2+f_y^2<1 \\ 0 & \text{for } f_x^2+f_y^2>1 \end{cases} \tag{4.42}$$

$$\tilde{\Psi}_{1i} = \begin{cases} 0 & \text{for } f_x^2+f_y^2<1 \\ \tilde{\zeta}_1 & \text{for } f_x^2+f_y^2>1 \end{cases} \tag{4.43}$$

$$\tilde{\Psi}_{2r} = \begin{cases} \tilde{\zeta}_2 & \text{for } f_x^2+f_y^2<1 \\ 0 & \text{for } f_x^2+f_y^2>1 \end{cases} \tag{4.44}$$

$$\tilde{\Psi}_{2i} = \begin{cases} 0 & \text{for } f_x^2+f_y^2<1 \\ \tilde{\zeta}_2 & \text{for } f_x^2+f_y^2>1 \end{cases} \tag{4.45}$$

$$\tilde{\Psi}_{3r} = \begin{cases} \tilde{\zeta}_3 & \text{for } f_x^2+f_y^2<1 \\ 0 & \text{for } f_x^2+f_y^2>1 \end{cases} \tag{4.46}$$

$$\tilde{\Psi}_{3i} = \begin{cases} 0 & \text{for } f_x^2+f_y^2<1 \\ \tilde{\zeta}_3 & \text{for } f_x^2+f_y^2>1 \end{cases} \tag{4.47}$$

$$\tilde{\Psi}_{4r} = \begin{cases} \tilde{\zeta}_4 & \text{for } f_x^2+f_y^2<1 \\ 0 & \text{for } f_x^2+f_y^2>1 \end{cases} \tag{4.48}$$

$$\tilde{\Psi}_{4i} = \begin{cases} 0 & \text{for } f_x^2 + f_y^2 < 1 \\ \tilde{\zeta}_4 & \text{for } f_x^2 + f_y^2 > 1 \end{cases} \tag{4.49}$$

$$\tilde{\Psi}_{5r} = \begin{cases} \tilde{\zeta}_5 & \text{for } f_x^2 + f_y^2 < 1 \\ 0 & \text{for } f_x^2 + f_y^2 > 1 \end{cases} \tag{4.50}$$

$$\tilde{\Psi}_{5i} = \begin{cases} 0 & \text{for } f_x^2 + f_y^2 < 1 \\ \tilde{\zeta}_5 & \text{for } f_x^2 + f_y^2 > 1 \end{cases} \tag{4.51}$$

$$\tilde{\Psi}_{6r} = \begin{cases} \tilde{\zeta}_6 & \text{for } f_x^2 + f_y^2 < 1 \\ 0 & \text{for } f_x^2 + f_y^2 > 1 \end{cases} \tag{4.52}$$

$$\tilde{\Psi}_{6i} = \begin{cases} 0 & \text{for } f_x^2 + f_y^2 < 1 \\ \tilde{\zeta}_6 & \text{for } f_x^2 + f_y^2 > 1 \end{cases} \tag{4.53}$$

where

$$\tilde{\zeta}_1 = (1 - f_x^2)d \tag{4.54}$$

$$\tilde{\zeta}_2 = -f_x f_y d \tag{4.55}$$

$$\tilde{\zeta}_3 = (1 - f_y^2)d \tag{4.56}$$

$$\tilde{\zeta}_4 = -(f_x^2 + f_y^2)d \tag{4.57}$$

$$\tilde{\zeta}_5 = f_x d \tag{4.58}$$

$$\tilde{\zeta}_6 = f_y d \tag{4.59}$$

The adjoint operators are computed from $\tilde{\Psi}_n^a = \tilde{\Psi}_n^*(-f_x, -f_y)$.

4.3 Surface Generation

The surface generation is based on the premise that any planar area may be approximated by a collection of square cells of dimension Δs. Arbitrary perimeter geometries may be generated by passing a spuare arroy of cell centroid locations through a series of constraints which determine whether the cell is inside or out-

side the perimeter. This information is then stored in a square tag array which represents a digital code for the geometry.

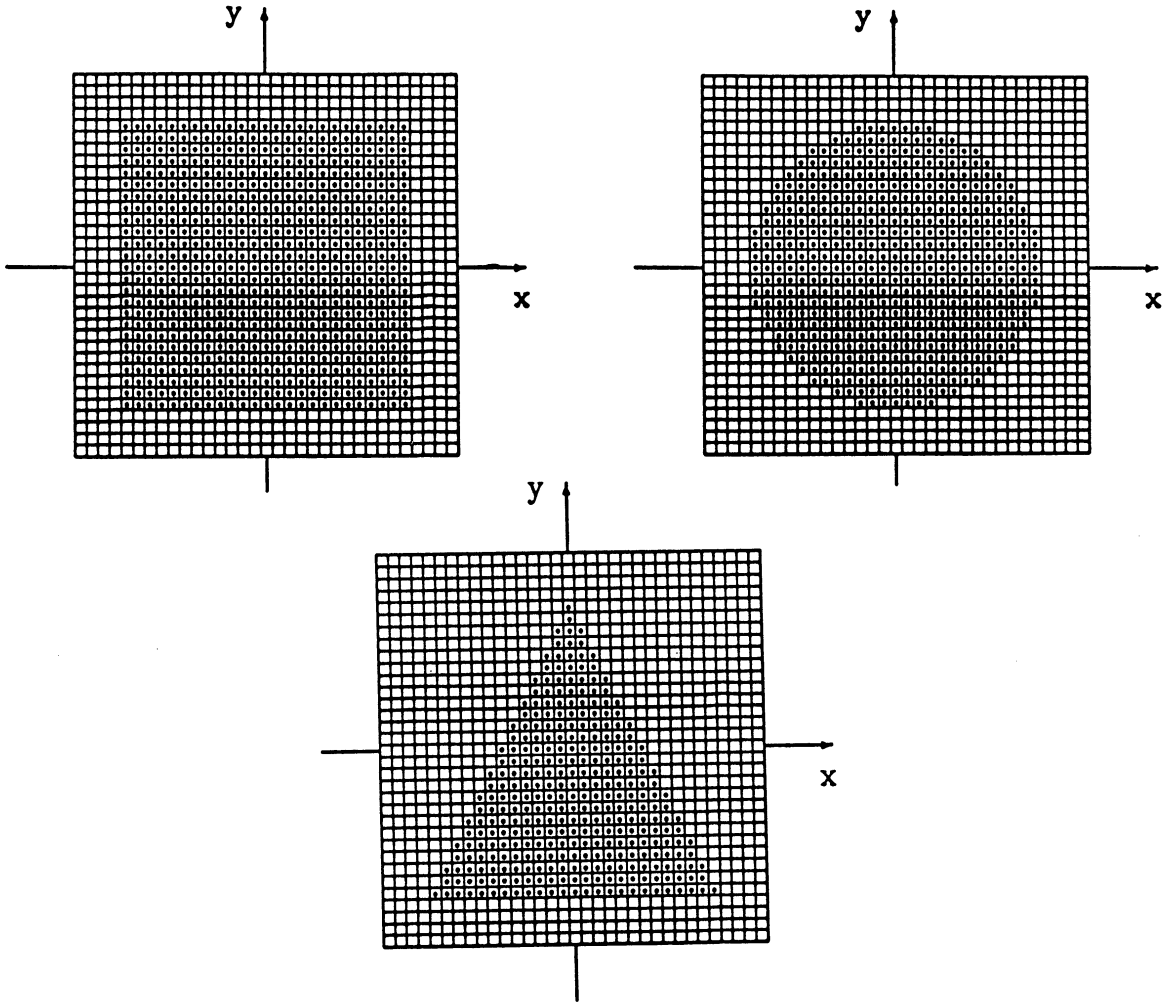

Figure 4.2. Digital Generation of a Square, Circular, or Triangular Plate.

4.4 Perfectly Conducting Plate

The program CGFCON solves for the surface current and the backscatter cross section of a planar perfectly conducting plate illuminated by a plane wave. At the present time the program is set up to allow circular, square and equilateral triangular perimeters. The unknown surface currents are found by solving a pair of coupled integral equations by a combined conjugate gradient FFT method.

4.4.1 Formulation and Implementation

The formulation for E-pol or H-pol results in two coupled integral equations which are defined and valid on the plate. Assume the coordinates are normalized to λ_0 and the current is normalized to Z_0^{-1}. The integral equations are

$$\iint_{S'} \left[\Psi_1 K_x^e + \Psi_2 K_y^e\right] dS' = E_x^i \tag{4.60}$$

$$\iint_{S'} \left[\Psi_2 K_x^e + \Psi_3 K_y^e\right] dS' = E_y^i \tag{4.61}$$

The plate is divided up into square cells of side Δ. The algorithm is given by

solve the 2 coupled equations for K_x^e and K_y^e

initialize

$$r_{x,y}^1 = E_{x,y}^i - \mathcal{F}^{-1}\left[\tilde{\Psi}_{1,2}\widetilde{K}_x^{e,0} + \tilde{\Psi}_{2,3}\widetilde{K}_y^{e,0}\right] \tag{4.62}$$

$$q_{x,y}^0 = \mathcal{F}^{-1}\left[\tilde{\Psi}_{1,2}^a \tilde{r}_x^1 + \tilde{\Psi}_{2,3}^a \tilde{r}_y^1\right] \tag{4.63}$$

$$\beta_0 = \left(|q_x^0|^2 + |q_y^0|^2\right)^{-1} \tag{4.64}$$

$$p_{x,y}^1 = \beta_0 q_{x,y}^0 \tag{4.65}$$

for $k = 1, \ldots$

$$q_{x,y}^k = \mathcal{F}^{-1}\left[\tilde{\Psi}_{1,2}\tilde{p}_x^k + \tilde{\Psi}_{2,3}\tilde{p}_y^k\right] \tag{4.66}$$

$$\alpha_k = \left(|q_x^k|^2 + |q_y^k|^2\right)^{-1} \tag{4.67}$$

$$K_{x,y}^{e,k+1} = K_{x,y}^{e,k} + \alpha_k p_{x,y}^k \tag{4.68}$$

$$r_{x,y}^{k+1} = r_{x,y}^k - \alpha_k q_{x,y}^k \tag{4.69}$$

$$q_{x,y}^{k+1} = \mathcal{F}^{-1}\left[\tilde{\Psi}_{1,2}^a \tilde{r}_x^{k+1} + \tilde{\Psi}_{2,3}^a \tilde{r}_y^{k+1}\right] \tag{4.70}$$

$$\beta_k = \left(|q_x^{k+1}|^2 + |q_y^{k+1}|^2\right)^{-1} \tag{4.71}$$

$$p_{x,y}^{k+1} = p_{x,y}^k + \beta_k q_{x,y}^{k+1} \tag{4.72}$$

terminate when

$$\frac{(|r_x^{k+1}|^2 + |r_y^{k+1}|^2)^{\frac{1}{2}}}{(|E_x^i|^2 + |E_y^i|^2)^{\frac{1}{2}}} < \text{tolerance} \tag{4.73}$$

The Algorithm is programmed by separating all parameters in to their real and imaginary parts. No complex numbers are explicitly used.

4.5 Thin Dielectric Plate

The program CGFDIE solves for the equivalent surface current and the backscatter cross section of a planar dielectric plate illuminated by a plane wave. The plate is assumed to be thin such that the thickness τ satisfies the relation $\tau << \lambda_p$ where λ_p is the wavelength inside the plate. At the present time the program is set up to allow circular, square and equilateral triangular perimeters. The unknown surface currents for the E-pol case are found by solving a pair of coupled integral equations by a combined conjugate gradient FFT method. The H-pol case requires the solution of an additional equation.

4.5.1 Formulation

The formulation for E-pol two coupled integral equations which are defined and valid on the plate. The H-pol case requires an additional solution for the normal component of current. Assume the coordinates are normalized to λ_0 and the current is normalized to Z_0^{-1}. The integral equations are given by

$$w_1 K_x^e + \iint_{S'} \left[\Psi_1 K_x^e + \Psi_2 K_y^e\right] dS' = E_x^i \tag{4.74}$$

$$w_1 K_y^e + \iint_{S'} \left[\Psi_2 K_x^e + \Psi_3 K_y^e\right] dS' = E_y^i \tag{4.75}$$

$$w_2 K_z^e - \iint_{S'} \Psi_4 K_z^e dS' = E_z^i \tag{4.76}$$

4.5.2 Implementation: E Polarization

The plate is divided up into square cells of side Δ. The algorithm for E-pol is given as

initialize

$$r^1_{x,y} = E^i_{x,y} - w_1 K^{e,0}_{x,y} - \mathcal{F}^{-1}\left[\tilde{\Psi}_{1,2}\widetilde{K}^{e,0}_x + \tilde{\Psi}_{2,3}\widetilde{K}^{e,0}_y\right] \quad (4.77)$$

$$q^0_{x,y} = w_1^* r^1_{x,y} + \mathcal{F}^{-1}\left[\tilde{\Psi}^a_{1,2}\tilde{r}^1_x + \tilde{\Psi}^a_{2,3}\tilde{r}^1_y\right] \quad (4.78)$$

$$\beta_0 = \left(|q^0_x|^2 + |q^0_y|^2\right)^{-1} \quad (4.79)$$

$$p^1_{x,y} = \beta_0 q^0_{x,y} \quad (4.80)$$

for $k = 1, \ldots$

$$q^k_{x,y} = w_1 p^k_{x,y} + \mathcal{F}^{-1}\left[\tilde{\Psi}_{1,2}\tilde{p}^k_x + \tilde{\Psi}_{2,3}\tilde{p}^k_y\right] \quad (4.81)$$

$$\alpha_k = \left(|q^k_x|^2 + |q^k_y|^2\right)^{-1} \quad (4.82)$$

$$K^{e,k+1}_{x,y} = K^{e,k}_{x,y} + \alpha_k p^k_{x,y} \quad (4.83)$$

$$r^{k+1}_{x,y} = r^k_{x,y} - \alpha_k q^k_{x,y} \quad (4.84)$$

$$q^{k+1}_{x,y} = w_1^* r^{k+1}_{x,y} + \mathcal{F}^{-1}\left[\tilde{\Psi}^a_{1,2}\tilde{r}^{k+1}_x + \tilde{\Psi}^a_{2,3}\tilde{r}^{k+1}_y\right] \quad (4.85)$$

$$\beta_k = \left(|q^{k+1}_x|^2 + |q^{k+1}_y|^2\right)^{-1} \quad (4.86)$$

$$p^{k+1}_{x,y} = p^k_{x,y} + \beta_k q^{k+1}_{x,y} \quad (4.87)$$

terminate when

$$\frac{(|r^{k+1}_x|^2 + |r^{k+1}_y|^2)^{\frac{1}{2}}}{(|E^i_x|^2 + |E^i_y|^2)^{\frac{1}{2}}} < \text{tolerance} \quad (4.88)$$

The Algorithm is programmed by separating all parameters in to their real and imaginary parts. No complex numbers are explicitly used.

4.5.3 Implementation: H Polarization

The H-pol case requires compution of the normal component of current in addition to the previous equations. The algorithm for the normal component of

current is

initialize

$$r_z^1 = E_z^i - w_2 K_z^{e,0} - \mathcal{F}^{-1}\left[\tilde{\Psi}_4 \widetilde{K}_z^{e,0}\right] \tag{4.89}$$

$$q_z^0 = w_2^* r_z^1 + \mathcal{F}^{-1}\left[\tilde{\Psi}_4^a \tilde{r}_z^1\right] \tag{4.90}$$

$$\beta_0 = |q_z^0|^{-2} \tag{4.91}$$

$$p_z^1 = \beta_0 q_z^0 \tag{4.92}$$

for $k = 1, \ldots$

$$q_z^k = w_2 p_z^k + \mathcal{F}^{-1}\left[\tilde{\Psi}_4 \tilde{p}_z^k\right] \tag{4.93}$$

$$\alpha_k = |q_z^k|^{-2} \tag{4.94}$$

$$K_z^{e,k+1} = K_z^{e,k} + \alpha_k p_z^k \tag{4.95}$$

$$r_z^{k+1} = r_z^k - \alpha_k q_z^k \tag{4.96}$$

$$q_z^{k+1} = w_2^* r_z^{k+1} + \mathcal{F}^{-1}\left[\tilde{\Psi}_4^a \tilde{r}_z^{k+1}\right] \tag{4.97}$$

$$\beta_k = |q_z^{k+1}|^{-2} \tag{4.98}$$

$$p_z^{k+1} = p_z^k + \beta_k q_z^{k+1} \tag{4.99}$$

terminate when

$$\frac{|r_z^{k+1}|}{|E_z^i|} < \text{tolerance} \tag{4.100}$$

Each Algorithm is programmed by separating all parameters in to their real and imaginary parts. No complex numbers are explicitly used. The more refined algorithm is given as

4.6 Thin Dielectric and Magnetic Plate

The program CGFDAM solves for the equivalent surface current and the backscatter cross section of a planar material plate composed of dielectric and magnetic

material illuminated by a plane wave. The plate is assumed to be thin such that the thickness τ satisfies the relation $\tau << \lambda_p$ where λ_p is the wavelength inside the plate. At the present time the program is set up to allow circular, square and equilateral triangular perimeters. The unknown surface currents are found by solving two sets of coupled integral equations by a combined conjugate gradient FFT method.

4.6.1 Formulation

Assume that the coordinates are normalized with respect to λ_0 and the electric currents are normalized by Z_0^{-1}. The E-pol equations are

$$w_1 K_x^e + \iint_{S'} \left[\Psi_1 K_x^e + \Psi_2 K_y^e + \Psi_6 K_z^m\right] dS' = E_x^i \tag{4.101}$$

$$w_1 K_y^e + \iint_{S'} \left[\Psi_2 K_x^e + \Psi_3 K_y^e - \Psi_5 K_z^m\right] dS' = E_y^i \tag{4.102}$$

$$w_4 K_z^m + \iint_{S'} \left[\Psi_6 K_x^e - \Psi_5 K_y^e - \Psi_4 K_z^m\right] dS' = H_z^i \tag{4.103}$$

$$w_2 K_x^m + \iint_{S'} \left[\Psi_1 K_x^m + \Psi_2 K_y^m\right] dS' = H_x^i \tag{4.104}$$

$$w_2 K_y^m + \iint_{S'} \left[\Psi_2 K_x^m + \Psi_3 K_y^m\right] dS' = H_y^i \tag{4.105}$$

and the H-pol equations are

$$w_2 K_x^m + \iint_{S'} \left[\Psi_1 K_x^m + \Psi_2 K_y^m - \Psi_6 K_z^e\right] dS' = H_x^i \tag{4.106}$$

$$w_2 K_y^m + \iint_{S'} \left[\Psi_2 K_x^m + \Psi_3 K_y^m + \Psi_5 K_z^e\right] dS' = H_y^i \tag{4.107}$$

$$w_2 K_z^e - \iint_{S'} \left[\Psi_6 K_x^m - \Psi_5 K_y^m + \Psi_4 K_z^e\right] dS' = E_z^i \tag{4.108}$$

$$w_1 K_x^e + \iint_{S'} \left[\Psi_1 K_x^e + \Psi_2 K_y^e\right] dS' = E_x^i \tag{4.109}$$

$$w_1 K_y^e + \iint_{S'} \left[\Psi_2 K_x^e + \Psi_3 K_y^e\right] dS' = E_y^i \tag{4.110}$$

4.6.2 Implementation: E-Polarization

The plate is divided up into square cells of side Δ. The algorithm for E-pol is solve the 3 coupled equations for K_x^e, K_y^e and K_z^m

initialize

$$r_{x,y}^1 = E_{x,y}^i - w_1 K_{x,y}^{e,1} - \mathcal{F}^{-1}\left[\tilde{\Psi}_{1,2}\widetilde{K}_x^{e,1} + \tilde{\Psi}_{2,4}\widetilde{K}_y^{e,1} \pm \tilde{\Psi}_{3,5}\widetilde{K}_z^{m,1}\right] \quad (4.111)$$

$$r_z^1 = H_z^i - w_2 K_z^{m,1} - \mathcal{F}^{-1}\left[\tilde{\Psi}_3\widetilde{K}_x^{e,1} - \tilde{\Psi}_5\widetilde{K}_y^{e,1} - \tilde{\Psi}_6\widetilde{K}_z^{m,1}\right] \quad (4.112)$$

$$q_{x,y}^0 = w_1^* r_{x,y}^1 + \mathcal{F}^{-1}\left[\tilde{\Psi}_{1,2}^a\tilde{r}_x^1 + \tilde{\Psi}_{2,4}^a\tilde{r}_y^1 \pm \tilde{\Psi}_{3,5}^a\tilde{r}_z^1\right] \quad (4.113)$$

$$q_z^0 = w_2^* r_z^1 + \mathcal{F}^{-1}\left[\tilde{\Psi}_3^a\tilde{r}_x^1 - \tilde{\Psi}_5^a\tilde{r}_y^1 - \tilde{\Psi}_6^a\tilde{r}_z^1\right] \quad (4.114)$$

$$\beta_0 = \left(|q_x^0|^2 + |q_y^0|^2 + |q_z^0|^2\right)^{-1} \quad (4.115)$$

$$p_{x,y,z}^1 = \beta_0 q_{x,y,z}^0 \quad (4.116)$$

$$(4.117)$$

for $k = 1, \ldots$

$$q_{x,y}^k = w_1 p_{x,y}^k + \mathcal{F}^{-1}\left[\tilde{\Psi}_{1,2}\tilde{p}_x^k + \tilde{\Psi}_{2,4}\tilde{p}_y^k \pm \tilde{\Psi}_{3,5}\tilde{p}_z^k\right] \quad (4.118)$$

$$q_z^k = w_2 p_z^k + \mathcal{F}^{-1}\left[\tilde{\Psi}_3\tilde{p}_x^k - \tilde{\Psi}_5\tilde{p}_y^k - \tilde{\Psi}_6\tilde{p}_z^k\right] \quad (4.119)$$

$$\alpha_k = \left(|q_x^k|^2 + |q_y^k|^2 + |q_z^k|^2\right) \quad (4.120)$$

$$K_{x,y}^{e,k+1} = K_{x,y}^{e,k} + \alpha_k p_{x,y}^k \quad (4.121)$$

$$K_z^{m,k+1} = K_z^{m,k} + \alpha_k p_z^k \quad (4.122)$$

$$r_{x,y,z}^{k+1} = r_{x,y,z}^k - \alpha_k q_{x,y,z}^k \quad (4.123)$$

$$q_{x,y}^{k+1} = w_1^* r_{x,y}^{k+1} + \mathcal{F}^{-1}\left[\tilde{\Psi}_{1,2}^a\tilde{r}_x^{k+1} + \tilde{\Psi}_{2,4}^a\tilde{r}_y^{k+1} \pm \tilde{\Psi}_{3,5}^a\tilde{r}_z^{k+1}\right] \quad (4.124)$$

$$q_z^{k+1} = w_2^* r_z^{k+1} + \mathcal{F}^{-1}\left[\tilde{\Psi}_3^a\tilde{r}_x^{k+1} - \tilde{\Psi}_5^a\tilde{r}_y^{k+1} - \tilde{\Psi}_6^a\tilde{r}_z^{k+1}\right] \quad (4.125)$$

$$\beta_k = \left(|q_x^{k+1}|^2 + |q_y^{k+1}|^2 + |q_z^{k+1}|^2\right)^{-1} \quad (4.126)$$

$$p_{x,y,z}^{k+1} = p_{x,y,z}^k + \beta_k q_{x,y,z}^{k+1} \quad (4.127)$$

terminate when

$$\frac{(|r_x^{k+1}|^2 + |r_y^{k+1}|^2 + |r_z^{k+1}|^2)^{\frac{1}{2}}}{(|E_x^i|^2 + |E_y^i|^2 + |H_z^i|^2)^{\frac{1}{2}}} \quad < \quad \text{tolerance} \tag{4.128}$$

solve the 2 coupled equations for K_x^m and K_y^m

initialize

$$r_{x,y}^1 = H_{x,y}^i - w_3 K_{x,y}^{m,1} - \mathcal{F}^{-1}\left[\tilde{\Psi}_{1,2}\widetilde{K}_x^{m,1} + \tilde{\Psi}_{2,4}\widetilde{K}_y^{m,1}\right] \tag{4.129}$$

$$q_{x,y}^0 = w_3^* r_{x,y}^1 + \mathcal{F}^{-1}\left[\tilde{\Psi}_{1,2}^a \tilde{r}_x^1 + \tilde{\Psi}_{2,4}^a \tilde{r}_y^1\right] \tag{4.130}$$

$$\beta_0 = \left(|q_x^0|^2 + |q_y^0|^2\right)^{-1} \tag{4.131}$$

$$p_{x,y}^1 = \beta_0 q_{x,y}^0 \tag{4.132}$$

for $k = 1, \ldots$

$$q_{x,y}^k = w_3 p_{x,y}^k + \mathcal{F}^{-1}\left[\tilde{\Psi}_{1,2}\tilde{p}_x^k + \tilde{\Psi}_{2,4}\tilde{p}_y^k\right] \tag{4.133}$$

$$\alpha_k = \left(|q_x^k|^2 + |q_y^k|^2\right)^{-1} \tag{4.134}$$

$$K_{x,y}^{m,k+1} = K_{x,y}^{m,k} + \alpha_k p_{x,y}^k \tag{4.135}$$

$$r_{x,y}^{k+1} = r_{x,y}^k - \alpha_k q_{x,y}^k \tag{4.136}$$

$$q_{x,y}^{k+1} = w_3^* r_{x,y}^{k+1} + \mathcal{F}^{-1}\left[\tilde{\Psi}_{1,2}^a \tilde{r}_x^{k+1} + \tilde{\Psi}_{2,4}^a \tilde{r}_y^{k+1}\right] \tag{4.137}$$

$$\beta_k = \left(|q_x^{k+1}|^2 + |q_y^{k+1}|^2\right)^{-1} \tag{4.138}$$

$$p_{x,y}^{k+1} = p_{x,y}^k + \beta_k q_{x,y}^{k+1} \tag{4.139}$$

terminate when

$$\frac{(|r_x^{k+1}|^2 + |r_y^{k+1}|^2)^{\frac{1}{2}}}{(|H_x^i|^2 + |H_y^i|^2)^{\frac{1}{2}}} \quad < \quad \text{tolerance} \tag{4.140}$$

Implimenting this algorithm is most efficient without use of any complex numbers.

4.6.3 Implementation: H-Polarization

The algorithm for the H-pol case is

solve the 3 coupled equations for K_x^m, K_y^m and K_z^e

initialize

$$r_{x,y}^1 = H_{x,y}^i - w_3 K_{x,y}^{m,1} - \mathcal{F}^{-1}\left[\tilde{\Psi}_{1,2}\widetilde{K}_x^{m,1} + \tilde{\Psi}_{2,4}\widetilde{K}_y^{m,1} \mp \tilde{\Psi}_{3,5}\widetilde{K}_z^{e,1}\right] \quad (4.141)$$

$$r_z^1 = E_z^i - w_4 K_z^{e,1} + \mathcal{F}^{-1}\left[\tilde{\Psi}_3\widetilde{K}_x^{m,1} - \tilde{\Psi}_5\widetilde{K}_y^{m,1} + \tilde{\Psi}_6\widetilde{K}_z^{e,1}\right] \quad (4.142)$$

$$q_{x,y}^0 = w_3^* r_{x,y}^1 + \mathcal{F}^{-1}\left[\tilde{\Psi}_{1,2}^a\tilde{r}_x^1 + \tilde{\Psi}_{2,4}^a\tilde{r}_y^1 \mp \tilde{\Psi}_{3,5}^a\tilde{r}_z^1\right] \quad (4.143)$$

$$q_z^0 = w_4^* r_z^1 - \mathcal{F}^{-1}\left[\tilde{\Psi}_3^a\tilde{r}_x^1 - \tilde{\Psi}_5^a\tilde{r}_y^1 + \tilde{\Psi}_6^a\tilde{r}_z^1\right] \quad (4.144)$$

$$\beta_0 = \left(|q_x^0|^2 + |q_y^0|^2 + |q_z^0|^2\right)^{-1} \quad (4.145)$$

$$p_{x,y,z}^1 = \beta_0 q_{x,y,z}^0 \quad (4.146)$$

for $k = 1, \ldots$

$$q_{x,y}^k = w_3 p_x^k + \mathcal{F}^{-1}\left[\tilde{\Psi}_{1,2}\tilde{p}_x^k + \tilde{\Psi}_{2,4}\tilde{p}_y^k \mp \tilde{\Psi}_{3,5}\tilde{p}_z^k\right] \quad (4.147)$$

$$q_z^k = w_4 p_z^k - \mathcal{F}^{-1}\left[\tilde{\Psi}_3\tilde{p}_x^k - \tilde{\Psi}_5\tilde{p}_y^k + \tilde{\Psi}_6\tilde{p}_z^k\right] \quad (4.148)$$

$$\alpha_k = \left(|q_x^k|^2 + |q_y^k|^2 + |q_z^k|^2\right) \quad (4.149)$$

$$K_{x,y}^{m,k+1} = K_{x,y}^{m,k} + \alpha_k p_{x,y}^k \quad (4.150)$$

$$K_z^{e,k+1} = K_z^{e,k} + \alpha_k p_z^k \quad (4.151)$$

$$r_{x,y,z}^{k+1} = r_{x,y,z}^k - \alpha_k q_{x,y,z}^k \quad (4.152)$$

$$q_{x,y}^{k+1} = w_3^* r_{x,y}^{k+1} + \mathcal{F}^{-1}\left[\tilde{\Psi}_{1,2}^a\tilde{r}_x^{k+1} + \tilde{\Psi}_{2,4}^a\tilde{r}_y^{k+1} \mp \tilde{\Psi}_{3,5}^a\tilde{r}_z^{k+1}\right] \quad (4.153)$$

$$q_z^{k+1} = w_4^* r_z^{k+1} - \mathcal{F}^{-1}\left[\tilde{\Psi}_3^a\tilde{r}_x^{k+1} - \tilde{\Psi}_5^a\tilde{r}_y^{k+1} + \tilde{\Psi}_6^a\tilde{r}_z^{k+1}\right] \quad (4.154)$$

$$\beta_k = \left(|q_x^{k+1}|^2 + |q_y^{k+1}|^2 + |q_z^{k+1}|^2\right)^{-1} \quad (4.155)$$

$$p_{x,y,z}^{k+1} = p_{x,y,z}^k + \beta_k q_{x,y,z}^{k+1} \quad (4.156)$$

terminate when

$$\frac{(|r_x^{k+1}|^2 + |r_y^{k+1}|^2 + |r_z^{k+1}|^2)^{\frac{1}{2}}}{(|H_x^i|^2 + |H_y^i|^2 + |E_z^i|^2)^{\frac{1}{2}}} < \text{tolerance} \quad (4.157)$$

solve the 2 coupled equations for K_x^e and K_y^e

initialize

$$r_{x,y}^1 = E_{x,y}^i - w_1 K_{x,y}^{e,1} - \mathcal{F}^{-1}\left[\tilde{\Psi}_{1,2}\widetilde{K}_x^{e,1} + \tilde{\Psi}_{2,4}\widetilde{K}_y^{e,1}\right] \quad (4.158)$$

$$q_{x,y}^0 = w_1^* r_{x,y}^1 + \mathcal{F}^{-1}\left[\tilde{\Psi}_{1,2}^a \tilde{r}_x^1 + \tilde{\Psi}_{2,4}^a \tilde{r}_y^1\right] \quad (4.159)$$

$$\beta_0 = \left(|q_x^0|^2 + |q_y^0|^2\right)^{-1} \quad (4.160)$$

$$p_{x,y}^1 = \beta_0 q_{x,y}^0 \quad (4.161)$$

for $k = 1, \ldots$

$$q_{x,y}^k = w_1 p_{x,y}^k + \mathcal{F}^{-1}\left[\tilde{\Psi}_{1,2}\tilde{p}_x^k + \tilde{\Psi}_{2,4}\tilde{p}_y^k\right] \quad (4.162)$$

$$\alpha_k = \left(|q_x^k|^2 + |q_y^k|^2\right)^2 \quad (4.163)$$

$$K_{x,y}^{e,k+1} = K_{x,y}^{e,k} + \alpha_k p_{x,y}^k \quad (4.164)$$

$$r_{x,y}^{k+1} = r_{x,y}^k - \alpha_k q_{x,y}^k \quad (4.165)$$

$$q_{x,y}^{k+1} = w_1^* r_x^{k+1} + \mathcal{F}^{-1}\left[\tilde{\Psi}_{1,2}^a \tilde{r}_x^{k+1} + \tilde{\Psi}_{2,4}^a \tilde{r}_y^{k+1}\right] \quad (4.166)$$

$$\beta_k = \left(|q_x^{k+1}|^2 + |q_y^{k+1}|^2\right) \quad (4.167)$$

$$p_{x,y}^{k+1} = p_{x,y}^k + \beta_k q_{x,y}^{k+1} \quad (4.168)$$

terminate when

$$\frac{(|r_x^{k+1}|^2 + |r_y^{k+1}|^2)^{\frac{1}{2}}}{(|E_x^i|^2 + |E_y^i|^2)^{\frac{1}{2}}} < \text{tolerance} \quad (4.169)$$

4.7 Calculation of Radar Cross Section

The scattered far zone electric field is given by

$$\bar{E}^s(R) = jk_0 G(R)[\hat{R} \times \bar{N}_t^m(\theta,\phi) - Z_0 \bar{N}_t^e(\theta,\phi)] \quad (4.170)$$

where $\bar{N}_t^{e,m}(\theta,\phi)$ has the θ and ϕ components

$$N_\theta^{e,m} = \cos(\theta)[\cos(\phi)S_x^{e,m}(\theta,\phi) + \sin(\phi)S_y^{e,m}(\theta,\phi)] - \sin(\theta)S_z^{e,m}(\theta,\phi)$$

$$N_\phi^{e,m} = -\sin(\phi)S_x^{e,m}(\theta,\phi) + \cos(\phi)S_y^{e,m}(\theta,\phi) \quad (4.171)$$

and

$$\bar{S}^{e,m}(\theta,\phi) = \iint_{S'} \bar{K}^{e,m}(\bar{r}')e^{jk_0(\bar{r}'\cdot\hat{r})}dS'. \tag{4.172}$$

If the current is constant over the square cell and the coordinates are normalized to λ_0 then

$$\bar{S}^{e,m}(\theta,\phi) = F(\theta,\phi)\sum_{p=1}^{n}\sum_{q=1}^{n}\bar{K}^{e,m}(p,q)e^{j2\pi\sin(\theta)[\cos(\phi)x(p)+\sin(\phi)y(q)]} \tag{4.173}$$

where

$$F(\theta,\phi) = \frac{1}{\pi^2}\frac{\sin\left[\pi\Delta\sin(\theta)\cos(\phi)\right]}{\sin(\theta)\cos(\phi)}\frac{\sin\left[\pi\Delta\sin(\theta)\sin(\phi)\right]}{\sin(\theta)\sin(\phi)}. \tag{4.174}$$

For the electric current normalized to Z_0^{-1} the backscatter cross section is given by

$$\begin{aligned}\sigma &= \lim_{R\to\infty} 4\pi R^2\frac{|\bar{E}^s|^2}{|\bar{E}^i|^2} \\ &= \pi\left[|N_\phi^m + N_\theta^e|^2 + |N_\theta^m - N_\phi^e|^2\right].\end{aligned} \tag{4.175}$$

CHAPTER V

RESULTS

The conjugate gradient FFT algorithms given in chapter V were implemented using the prime factorization described in chapter III. This allowed an efficient solution of all plate shapes and sizes. In addition, the FFT employed was specialized to exploit the sparcity of the data due to the zero padding. An additional increase in the convergence rate was observed combining the higher order integration formulas with the prime factor FFT. The total computational time was reduced by a factor of 3 to 4 over the authors previous programs using a conventional Cooley-Tukey mixed radix FFT.

Figures 5.1-5.4 show the magnitude of the induced surface current on a square perfectly conducting plate illuminated by a plane wave at normal and edge-on incidence. Figures 5.5-5.8 compare computed backscatter patterns with experimental mesurements for a perfectly conducting triangular plate and a RAM material square plate. Figures 5.9-5.10 compare computed results with a semi-analytical method by Chu et al [24] for a circular dielectric plate. Figure 5.11 compares the computed backscatter pattern of a square constant 1 ohm resistive plate with a quadratically tapered plate with 1 ohm at the center and $5Z_0$ at the edges.

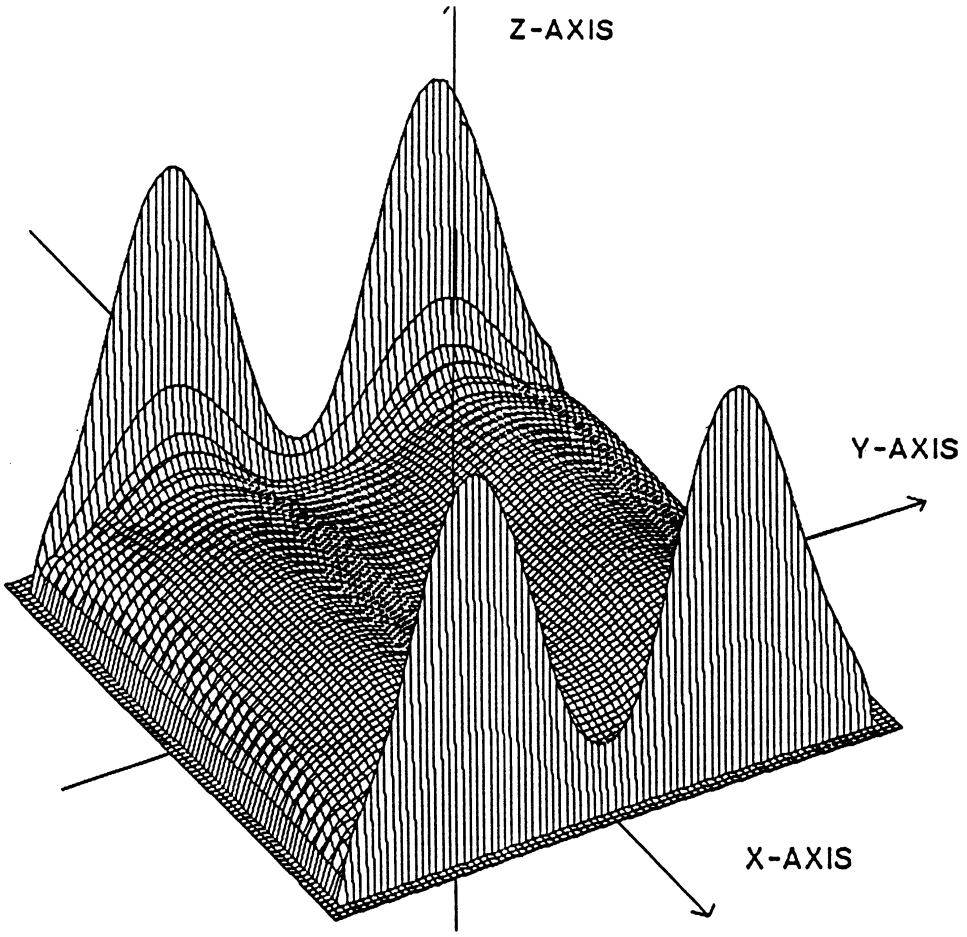

Figure 5.1. $|K_y^e|$:perfectly conducting plate,$s = 2\lambda_0, \Delta = \frac{2}{77}\lambda_0, tol = .007, iter = 500, n = 256, \theta = 0°, \phi = 0°, scale = 1.0.$

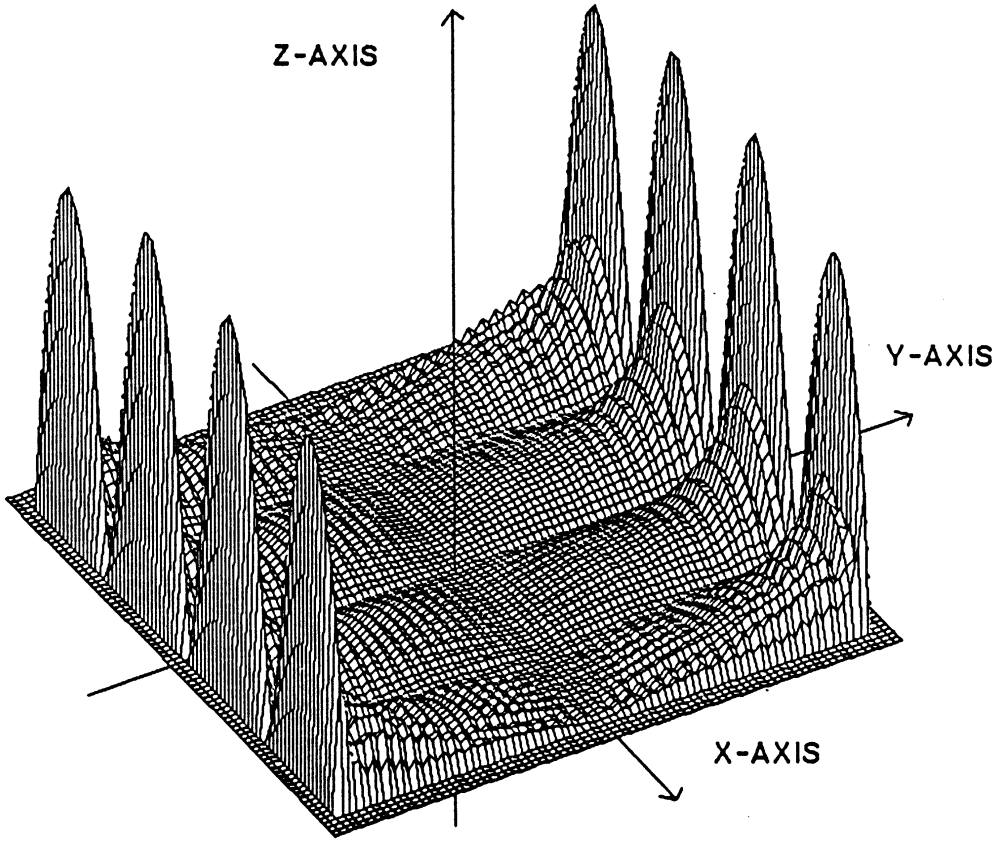

Figure 5.2. $|K_x^e|$:perfectly conducting plate,$s = 2\lambda_0, \Delta = \frac{2}{77}\lambda_0, tol = .007, iter = 500, n = 256, \theta = 0°, \phi = 0°, scale = 6.1.$

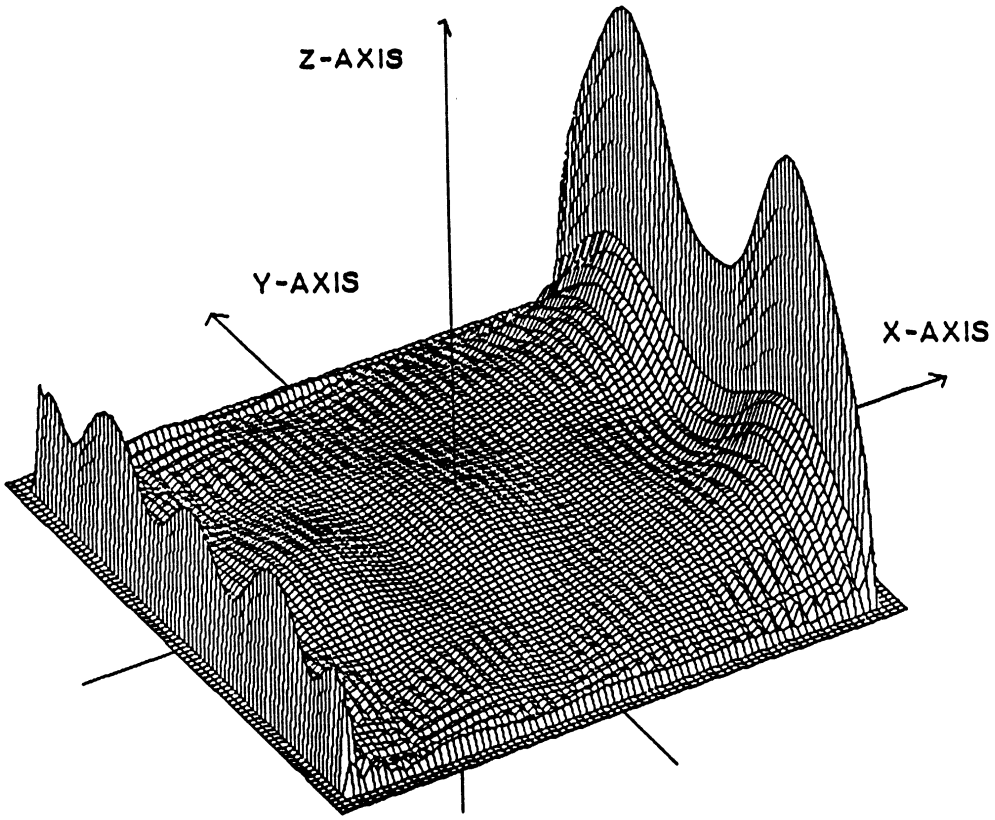

Figure 5.3. $|K_y^e|$:perfectly conducting plate,$s = 2\lambda_0, \Delta = \frac{2}{77}\lambda_0, tol = .007, iter = 500, n = 256, \theta = 90°, \phi = 0°, scale = 1.0.$

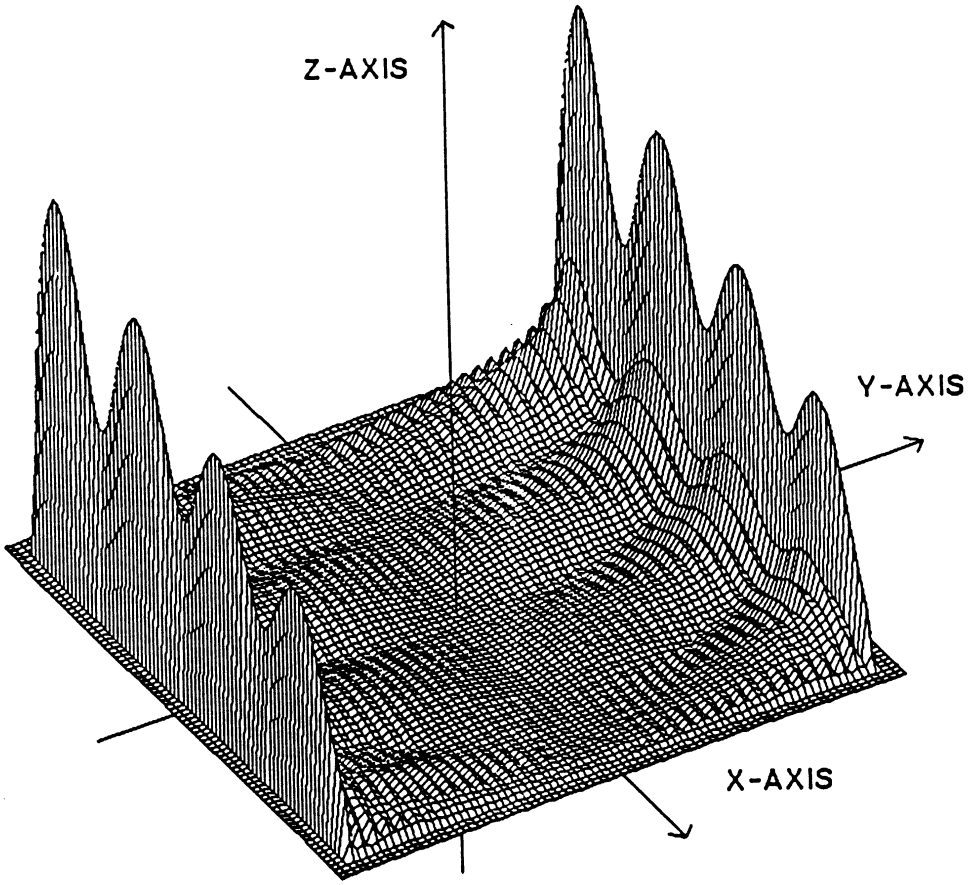

Figure 5.4. $|K_x^e|$:perfectly conducting plate,$s = 2\lambda_0, \Delta = \frac{2}{77}\lambda_0, tol = .007, iter = 500, n = 256, \theta = 90°, \phi = 0°, scale = 0.8.$

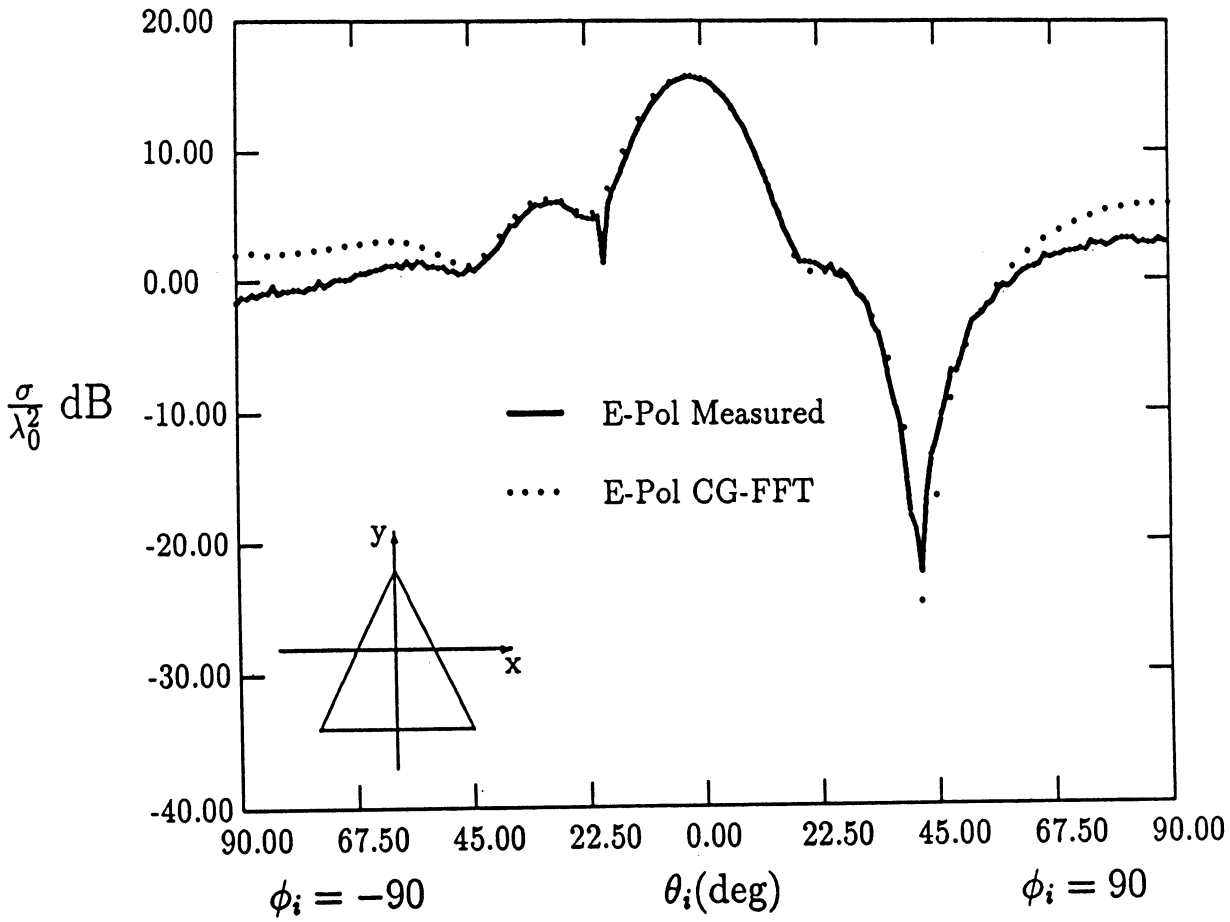

Figure 5.5. Perfectly conducting equilateral triangular plate: $y - zplane, s = 2\lambda_0, tol = .05, \Delta = \frac{2}{39}\lambda_0, n = 128.$

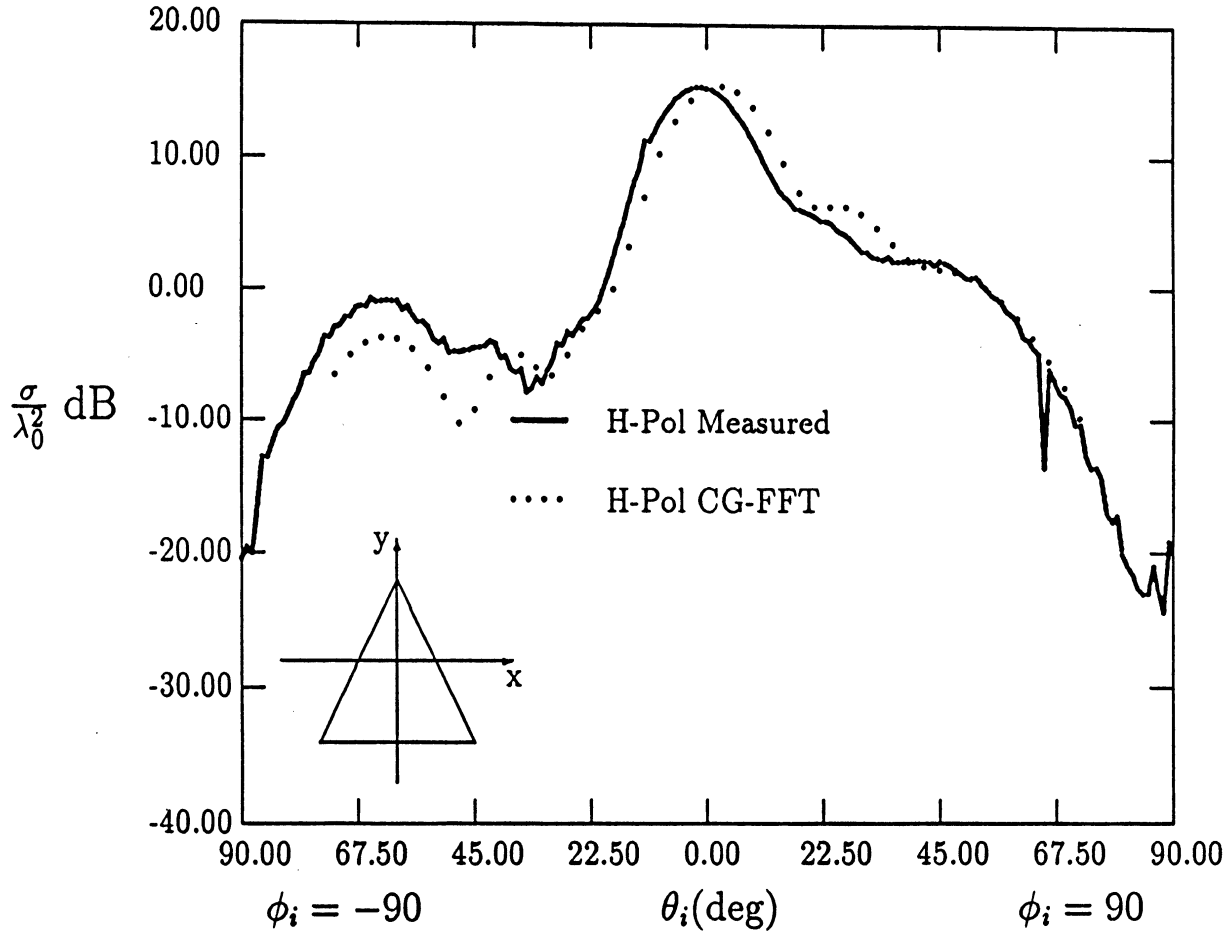

Figure 5.6. Perfectly conducting equilateral triangular plate: $y - zplane, s = 2\lambda_0, tol = .05, \Delta = \frac{2}{39}\lambda_0, n = 128.$

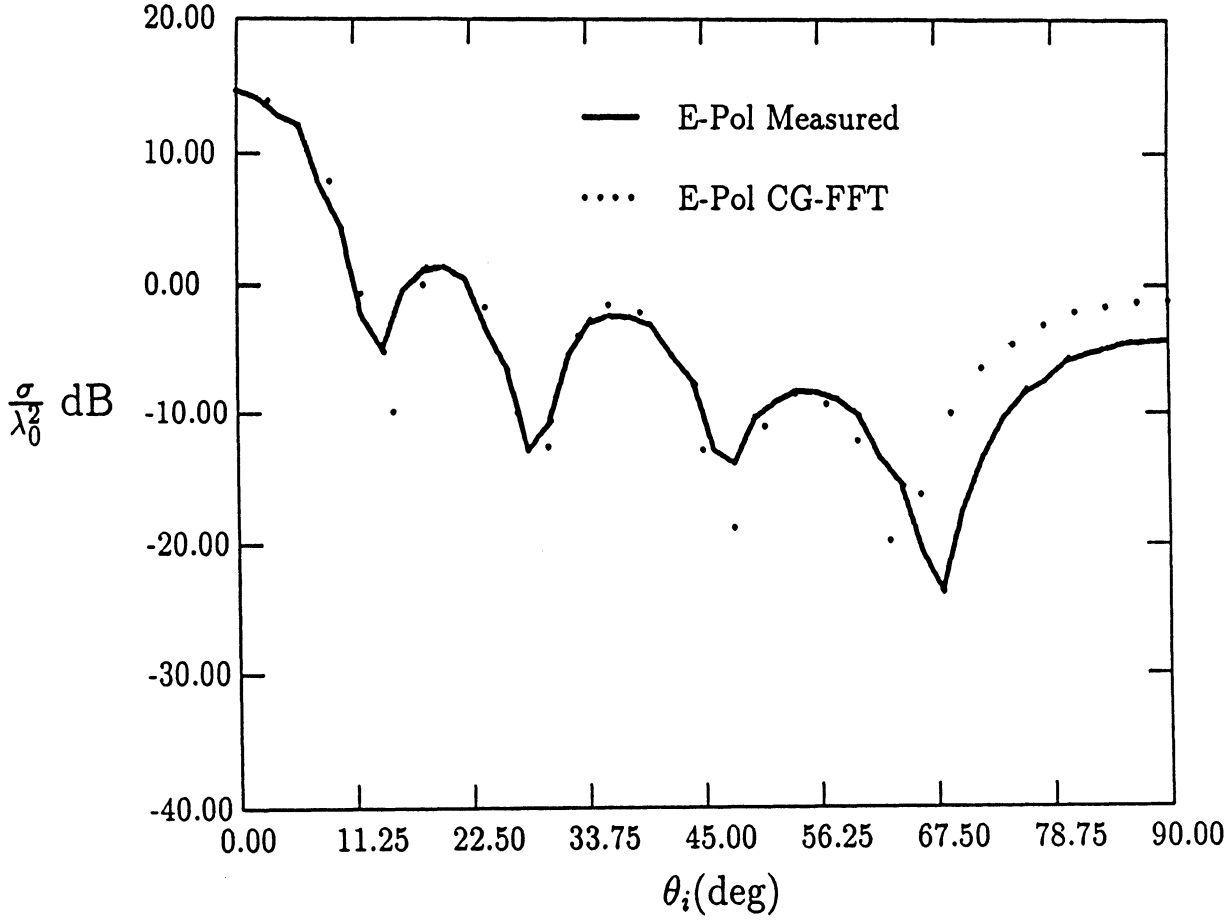

Figure 5.7. Square plate: $s = 2\lambda_0$,$\tau = .0254\lambda_0$, $\epsilon_r = 7.4 - j1.11$,$\mu_r = 1.4 - j0.672$,$tol = .001$,$\Delta = \frac{2}{39}\lambda_0$, n=128.

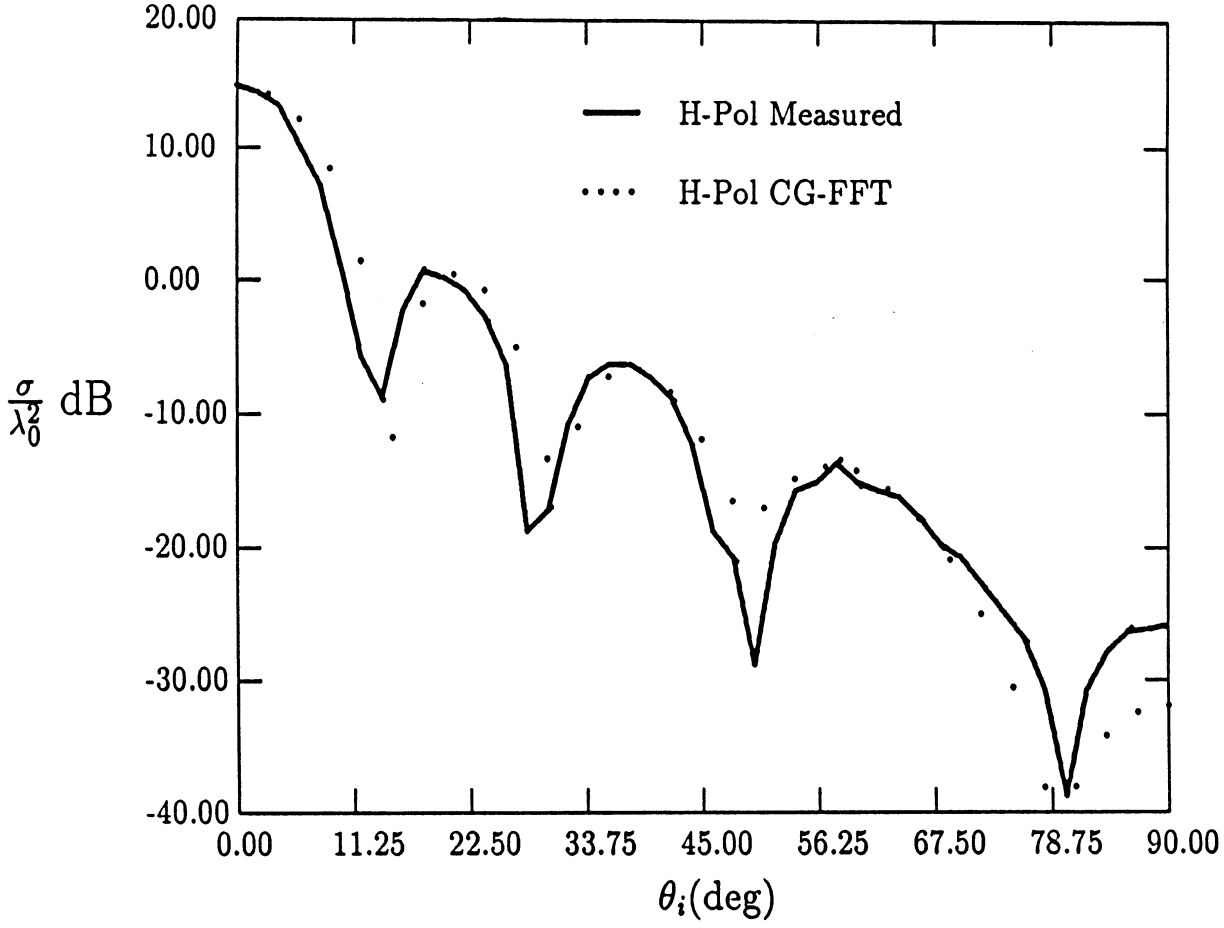

Figure 5.8. Square plate: $s = 2\lambda_0$,$\tau = .0254\lambda_0$, $\epsilon_r = 7.4 - j1.11$,$\mu_r = 1.4 - j0.672$,$tol = .001$,$\Delta = \frac{2}{39}\lambda_0$, n=128.

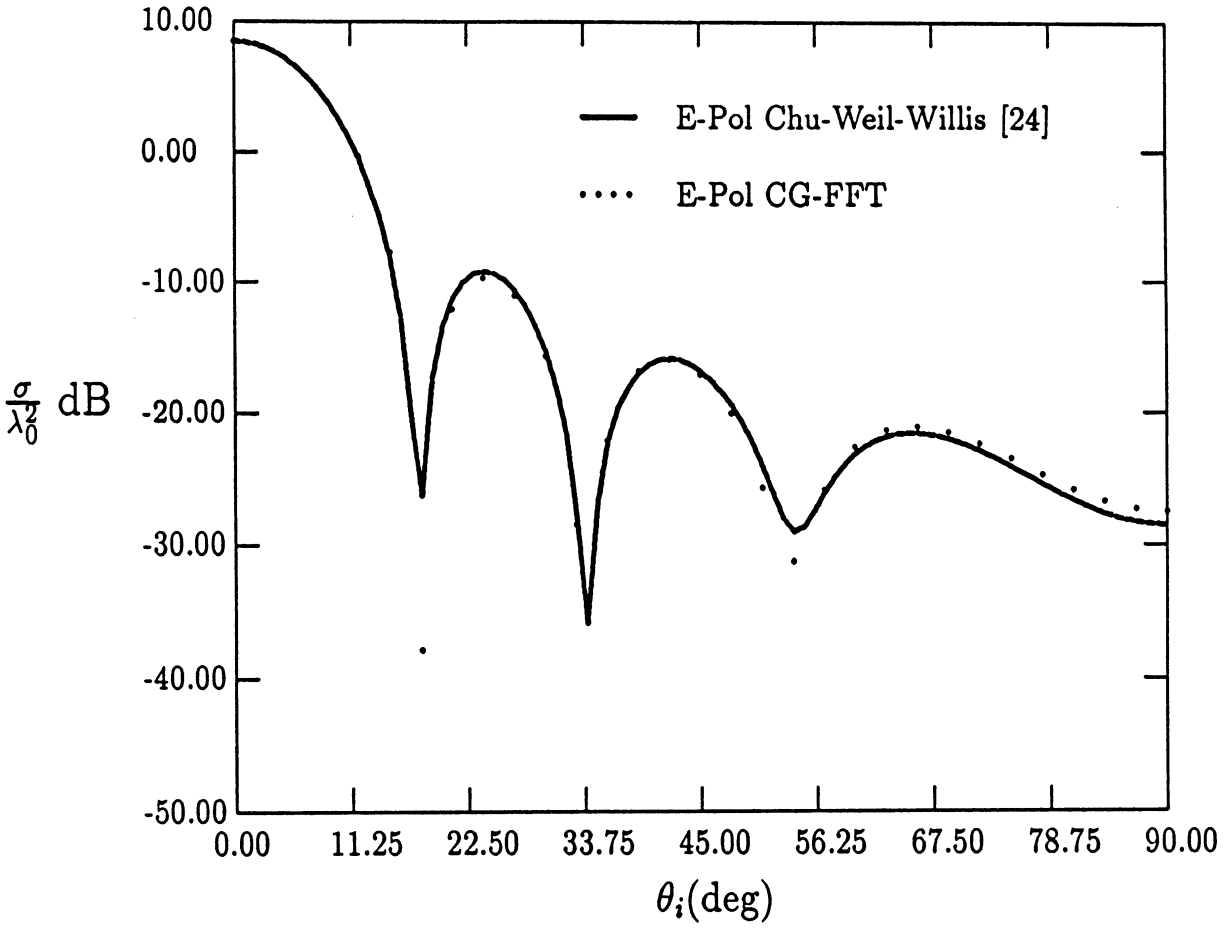

Figure 5.9. Circular plate: $r_0 = \lambda_0, \tau = .01\lambda_0$, $\epsilon_r = 2.0 - j10.0, tol = .001, \Delta = \frac{2}{39}\lambda_0$, n=128.

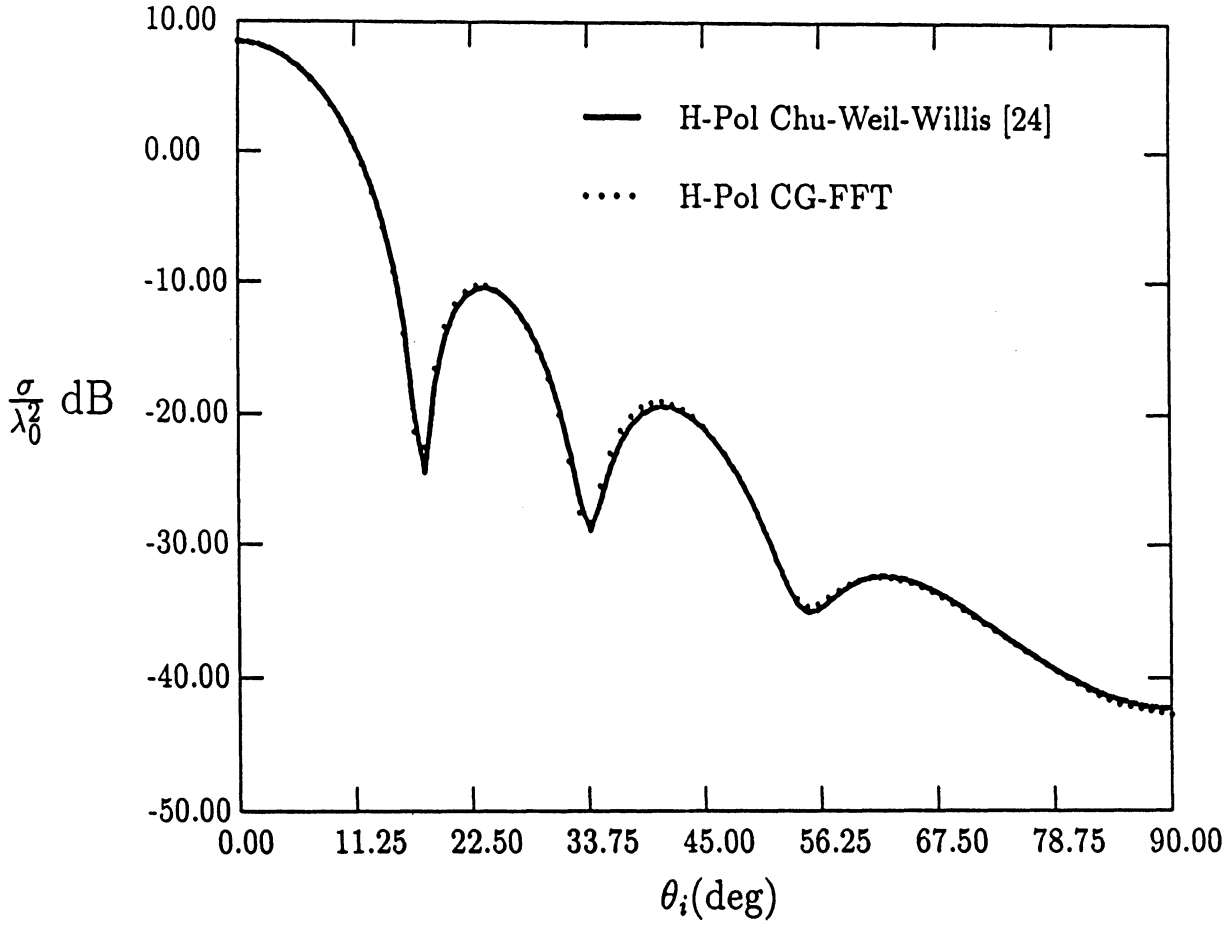

Figure 5.10. Circular plate: $r_0 = \lambda_0$,$\tau = .01\lambda_0$, $\epsilon_r = 2.0 - j10.0$,$tol = .001$,$\Delta = \frac{2}{39}\lambda_0$, n=128.

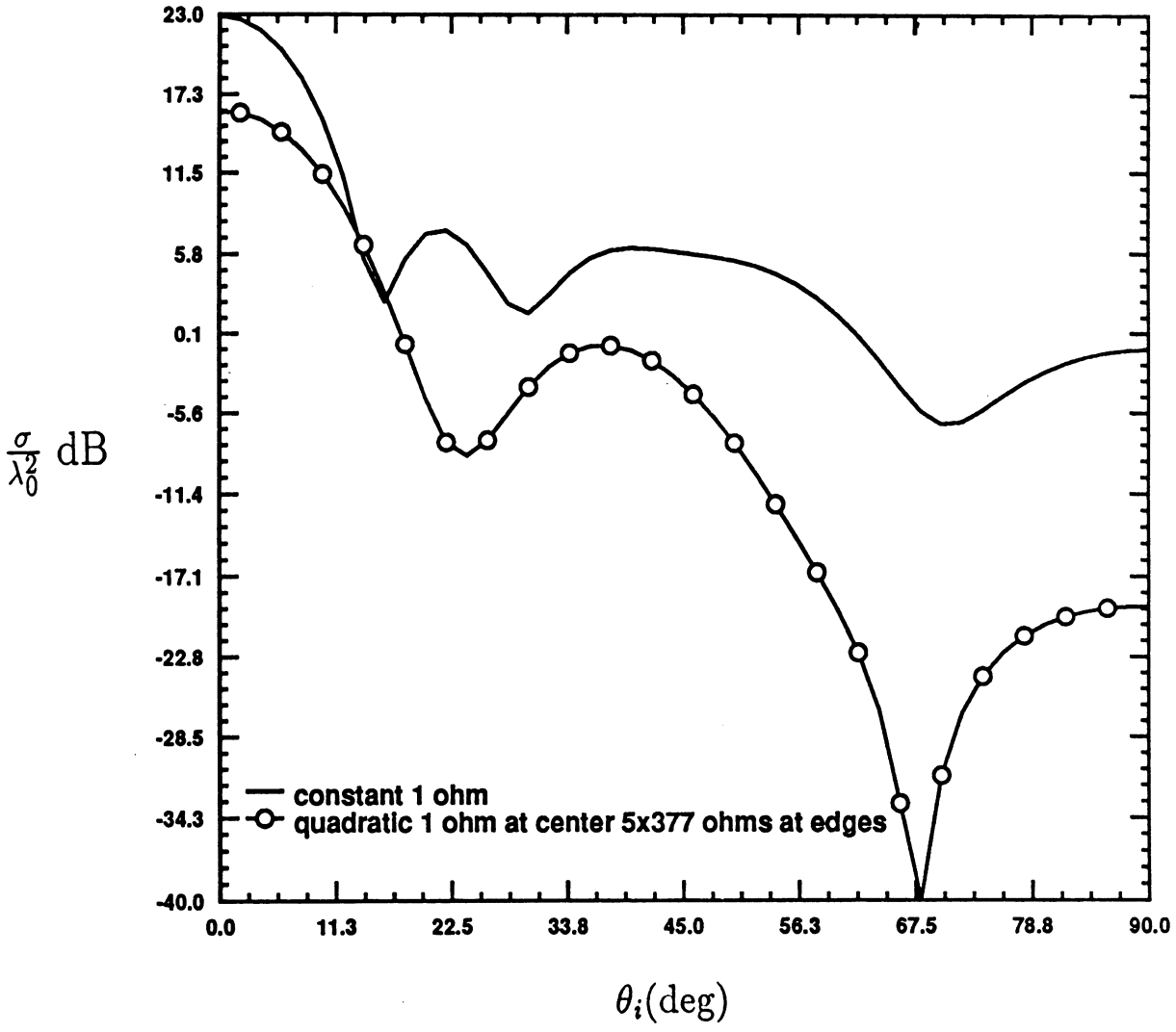

Figure 5.11. Square resistive plate:$s = 2\lambda_0$,$\tau = .01\lambda_0$, $tol = .001$,$\Delta = \frac{2}{35}\lambda_0$, n=72.

CHAPTER VI

FUTURE WORK

There are basically three projects under consideration for the near future which are extensions of the ideas presented in the previous chapters. They are

1 scattering by multiple layer planar plates

2 scattering by single and multiple layer non-planar plates

3 synthesis of material tapers for different plate configurations

Project 1 is a direct extension of the techniques presented in the previous chapters. Project 2 concerns the development of a method which combines the versatility of a finite element method with the efficiency of a conjugate gradient method to solve scattering by non-planar plates. Project 3 assumes the material distribution of a plate is an unknown and solves the scattering problem for not only currents but also constitutive parameters such as ϵ and μ subject to certain constraints on the radiation pattern.

BIBLIOGRAPHY

BIBLIOGRAPHY

[1] E. H. Newman and M. R. Schrote, "An open integral formulation for electromagnetic scattering by material plates",IEEE Trans. Antennas Propagat., vol. AP-32,No. 7 ,July, 1984, pp. 672-678.

[2] M. Naor and T. B. A. Senior, "Scattering by resistive plates",Technical report no. 018803-1-T, Radiation Lab., Dept. of EECS, The University of Michigan, Sept., 1981.

[3] A. W. Glisson and D. R. Wilton, "Simple and efficient numerical methods for problems of electromagnetic radiation and scattering from surfaces",IEEE Trans. Antennas Propagat., vol. AP-28,No. 5 ,Sept., 1980, pp. 593-603.

[4] S. M. Rao, D. M. Wilton,and A. W. Glisson, "Electromagnetic scattering by surfaces of arbitrary shape",IEEE Trans. Antennas Propagat., vol. AP-30,No. 3 ,May, 1982, pp. 409-418.

[5] T. K. Sarkar,E. Arvas and S. M. Rao, "Application of FFT and the conjugate gradient method for the solution of electromagnetic radiation from electrically large and small conducting bodies",IEEE Trans. Antennas Propagat., vol. AP-34, May, 1986, pp. 635-640.

[6] C. G. Christodoulou and J. F. Kauffman, "On the electromagnetic scattering from infinite rectangular grids with finite conductivity ",IEEE Trans. Antennas Propagat., vol. AP-34, Feb., 1986, pp. 144-154.

[7] M. R. Hestenes and E. Steifel, "Method of conjugate gradients for solving linear systems", J. Res. Nat. Bur. Standard., vol. 49, no. 6, Dec., 1952,

pp.409-436.

[8] M. R. Hestenes, "Conjugate direction methods in optimization", New York, Springer-Verlag,1980.

[9] J. W. Daniel, "The conjugate gradient method for linear and nonlinear operator equations",Siam J. Numer. Anal., vol. 4, no. 1, 1967, pp. 10-26.

[10] J. W. Golub, and C. F. VanLoan, "Matrix computions", John Hopkins University Press, Baltimore, MD, 1983, pp. 363-379.

[11] IEEE, "Special issue on the fast fourier transform and its application to digital filtering and spectral analysis",IEEE Trans. on Audio and Electroacoustics, Vol. AU-15, No.2, June, 1967.

[12] M. T. Heideman and C. S. Burrus, "A Bibliography of Fast Transform and Convolution Algorithms II", Technical Report No. 8402, Dept. of Elec. Engin., Rice University, Houston, Texas, Feb. 24, 1984.

[13] R. A. Horn, and C. A. Johnson, "Matrix analysis", Cambridge University Press, London, 1985, ch. 4,7.

[14] D. C. Champeney, "A Handbook of Fourier Theorems", Camgridge University Press, Cambridge Cb2 1rp, 1987.

[15] P. J. Davis and P. Rabinowitz, "Methods of Numerical Integration", 2nd Ed. Academic Press ,pp. 51-198, 1984.

[16] R. W. Hamming, "Numerical Methods for Scientists and Engineers", 2nd Ed. McGraw-Hill, pp. 277-316., 1973.

[17] J. W. Cooley and J. W. Tukey, "An Algorithm for the Machine Calculation of Complex Fourier Series", Math. of Comput., Vol. 19, pp. 297-301. April 1985.

[18] E. O. Brigham, "The Fast Fourier Transform", Prentice-Hall, Englewood Cliffs, NJ, pp. 191-195, 1974.

[19] D. T. Long, "Elementary Introduction to Number Theory", 3rd Ed., Prentice-Hall, Englewood Cliffs, NJ,pp. 117-123, 1987.

[20] I. J. Good, "The Relationship Between Two Fast Fourier Transforms", IEEE Trans. Computers, March 1971, pp. 310-317.

[21] C. Temperton, "Implementation of a Self-Sorting In-Place Prime Factor FFT Algorithm", J. Comput. Phys., 58, pp. 283-299, 1985.

[22] J. H. Rothweiler, "Implementation of the In-Order Prime Factor Transform for Variable Sizes", IEEE Trans. Acoust., Speech, Signal Processing, vol. ASSP-30, no. 1, Aug. 1982, pp. 105-107.

[23] C. S. Burrus and P. W. Eschenbacher, "An In-Place, In-Order Prime Factor FFT Algorithm", IEEE Trans. Acoust., Speech, Signal Processing, vol. ASSP-29, no. 4, Aug. 1981, pp. 806-817.

[24] T. M. Willis and H. Weil, "Disc scattering and absorption by an improved computational method", Applied Optics, Vol. 26, No. 18, pp. 3987-3995, 1987.